NASA TECHNICAL NOTE

NASA TN D-8305

EFFECT OF SIMULATED FORWARD AIRSPEED ON SMALL-SCALE-MODEL EXTERNALLY BLOWN FLAP NOISE

Jack H. Goodykoontz, Robert G. Dorsch, and William A. Olsen

Lewis Research Center
Cleveland, Ohio 44135

NATIONAL AERONAUTICS AND SPACE ADMINISTRATION • WASHINGTON, D. C. • SEPTEMBER 1976

Completed
13Apr77 lm

ERRATA

NASA Technical Note D-8305

EFFECT OF SIMULATED FORWARD AIRSPEED ON SMALL-SCALE-MODEL EXTERNALLY BLOWN FLAP NOISE

Jack H. Goodykoontz, Robert G. Dorsch, and William A. Olsen

September 1976

Page 56, figure 54: The legends for parts (a) and (b) should be reversed; that is, the the upper plot, (b), applies for takeoff conditions, and the lower plot, (a), for approach conditions.

Issued March 1977

1. Report No. NASA TN D-8305	2. Government Accession No.	3. Recipient's Catalog No.
4. Title and Subtitle EFFECT OF SIMULATED FORWARD AIRSPEED ON SMALL-SCALE-MODEL EXTERNALLY BLOWN FLAP NOISE		5. Report Date September 1976 6. Performing Organization Code
7. Author(s) Jack H. Goodykoontz, Robert G. Dorsch, and William A. Olsen		8. Performing Organization Report No. E-8697 10. Work Unit No. 505-05
9. Performing Organization Name and Address Lewis Research Center National Aeronautics and Space Administration Cleveland, Ohio 44135		11. Contract or Grant No. 13. Type of Report and Period Covered Technical Note
12. Sponsoring Agency Name and Address National Aeronautics and Space Administration Washington, D.C. 20546		14. Sponsoring Agency Code
15. Supplementary Notes		

16. Abstract

Noise tests were conducted on a small-scale model of an externally blown flap lift augmentation system. The nozzle/wing model was subjected to external flow that simulated takeoff and landing flight velocities by placing it in a 33-centimeter-diameter free jet. The results showed that external flow attenuated the noise associated with the various configurations tested. The amount of attenuation depended on flap setting. More attenuation occurred with a trailing-flap setting of 20^{o} than with one of 60^{o} Noise varied with relative velocity as a function of the trailing-flap setting and the angle from the nozzle inlet.

17. Key Words (Suggested by Author(s)) Acoustics; Aerodynamic noise; Aircraft noise; Flight simulation; Jet aircraft noise; Lift augmentation; Noise (sound); Short takeoff aircraft; Wing flaps	18. Distribution Statement Unclassified - unlimited STAR Category 02		
19. Security Classif. (of this report) Unclassified	20. Security Classif. (of this page) Unclassified	21. No. of Pages 57	22. Price* $4.50

* For sale by the National Technical Information Service, Springfield, Virginia 22161

EFFECT OF SIMULATED FORWARD AIRSPEED ON SMALL-SCALE-MODEL EXTERNALLY BLOWN FLAP NOISE

by Jack H. Goodykoontz, Robert G. Dorsch, and William A. Olsen

Lewis Research Center

SUMMARY

Noise tests were conducted on a small-scale model of an externally blown flap lift augmentation system by subjecting it to external flow that simulated takeoff and landing flight velocities. External flow was achieved by placing the nozzle/wing model in a 33-centimeter-diameter free jet. The test configurations consisted of a 5.08-centimeter-diameter conical nozzle, an eight-tube mixer nozzle with an equivalent diameter of 3.98 centimeters, and a wing model (chord length, 32.4 cm) with two flaps that could be set at various angles relative to the wing chord line. Test-nozzle jet velocities ranged from 208 to 340 meters per second, and external flow velocities from 0 to 79 meters per second.

The results showed that external flow attenuated the noise from the various configurations over the range of conditions investigated. The amount of attenuation depended on flap setting. That is, more attenuation occurred for a trailing-flap setting of 20° than for a more highly deflected flap setting of 60°. Noise radiation patterns were essentially unaffected by external flow. Noise varied with relative velocity (nozzle jet velocity minus external flow velocity) as a function of the trailing-flap setting and the angle from the nozzle inlet.

Data for the nozzles alone showed that external flow also attenuated the jet exhaust noise. Over the range of velocities tested, the total sound power of the nozzles varied as the sixth power of relative velocity.

INTRODUCTION

A number of experimental model studies have been made to determine the noise-generating characteristics of short-takeoff-and-landing (STOL) aircraft employing an

externally blown flap (EBF) lift augmentation system with lower surface blowing (refs. 1 to 5). The results have shown that flap noise is proportional to the sixth power of peak flap impingement velocity, so a slight increase in impingement velocity causes a substantial rise in flap noise. The experimental results presented in references 1 to 5 were obtained under static conditions, and thus the effect of flight velocity was not established.

Additional experimental work reported in reference 6 on peak-velocity decay rates from various nozzle configurations showed that forward velocity tends to decrease the decay rate of the jet exhaust. This implies an increase in flap noise for an EBF system as a result of the higher impingement velocity. Conversely, however, the jet exhaust noise was attenuated when the nozzles were subjected to forward airspeed. Therefore, the net effect of forward velocity on the noise signature of an EBF system remained to be determined.

This report presents the results of an experimental program that was undertaken to investigate the effect of simulated forward airspeed on the acoustic characteristics of an EBF system model.

Flow from a large conical nozzle (33-cm diam) was used to supply the external flow field to the test models. The test nozzle/wing models were mounted downstream of the exit of the large nozzle and centered on its axis. The test configurations consisted of a conical nozzle (5.08-cm diam), an eight-tube mixer nozzle (3.98-cm equivalent diam), and a model of a wing with two flaps that could be placed in various settings relative to the wing chord line (32.4-cm chord length with flaps retracted).

APPARATUS AND PROCEDURE

Airflow System

The airflow system (fig. 1) consisted essentially of a source of high-pressure air, flow throttling valves, mufflers, and the nozzles. Dry, cold air (280 to 300 K) was supplied to the 40.6-centimeter-diameter gate shutoff valve from a high-pressure air supply system (1.03×10^6 N/m^2 max.) by way of a 60.9-centimeter-diameter underground pipeline. Downstream of the gate shutoff valve the piping branched into two lines. One line consisted of a 10.2-centimeter-diameter pipe that supplied air to the small test nozzle that simulated the jet engine flow. The flow from the small nozzle was high velocity (200 to 340 m/sec). A globe valve was used to control the flow rate. A perforated plate with an open area of 20 percent was mounted in the 10.2-centimeter line downstream of the globe valve to eliminate low-frequency valve noise. Two mufflers downstream of the perforated plate attenuated the high-frequency noise caused by

flow through the plate. The first muffler was a tank with internal baffles that created a tortuous path for the flow. The interior surface of the tank and all surfaces of the baffles were lined with acoustically absorbent material. The second muffler was located farther downstream and consisted of a 20.32-centimeter-diameter pipe acoustically lined on its interior surface.

The second flow line downstream of the gate shutoff valve led to a 25.4-centimeter-diameter butterfly valve. The butterfly valve was used to control the flow through the large nozzle (free jet) that simulated forward velocity for the test models. The muffler system for this portion of the facility consisted of perforated plates and dissipative mufflers and is described in detail in references 1, 4, and 5.

The centerlines of the small and large nozzles were coincident and located 3.91 meters above grade.

Test Models

Two different nozzles for engine simulation were used in this program; a 5.08-centimeter-diameter conical nozzle and an eight-tube mixer nozzle with an equivalent diameter of 3.98 centimeters. The conical-nozzle/wing combination was a scaled-down version (scale factor, 6.5) of the apparatus described in reference 1. Further, the large-scale model of reference 1 was based on one of the designs for an EBF configuration described in references 7 and 8. For the mixer-nozzle/wing combination it was arbitrarily decided to maintain approximately the same ratio of X_i/D (or X_i/D_e for the mixer nozzle as was used for the conical-nozzle/wing combination. This ratio was 7.24 for the conical nozzle and 7.08 for the mixer nozzle. (All symbols are defined in the appendix.)

The test installation with the 5.08-centimeter-diameter conical nozzle in place is shown in figure 2. The test setup for this nozzle/wing model is shown in figure 3. The nozzle was attached to the 10.2-centimeter-diameter supply line concentrically with the 33-centimeter-diameter convergent nozzle (fig. 3(a)). The exit plane of the 5.08-centimeter-diameter nozzle was 22.8 centimeters downstream of the exit of the larger nozzle.

The wing had two flaps that were adjusted to any of three combinations of angle settings with respect to the wing chord line (1) 10°-20°, (2) 30°-60°, and (3) 0° (retracted). The wing had a span of 61 centimeters and a chord length of 32.4 centimeters with the flaps retracted. The leading edge of the wing was 6.06 centimeters downstream of the exit of the 5.08-centimeter-diameter nozzle and 9.15 centimeters above the nozzle axis. Thus, the wing passed entirely through the flow field of the free jet. The wing chord line was set at a 5° angle of attack relative to the nozzle axis

and was mounted with the spanwise direction in a vertical plane. Details of the conical nozzle are shown in figure 3(b).

The eight-tube mixer nozzle installed in the facility is shown in figure 4. Figure 5(a) gives the test setup for this nozzle/wing model. The mixer-nozzle exit was 31.40 centimeters downstream of the exit of the 33-centimeter-diameter nozzle and 2.54 centimeters downstream of the leading edge of the wing. Again, the leading edge of the wing was 9.15 centimeters above the axis of the nozzle, and the wing chord line was set at a 5° angle of attack relative to the nozzle axis. Figure 5(b) gives the details of the mixer nozzle. The nozzle had eight 1.41-centimeter-diameter tubes equally spaced on an 8-centimeter-diameter circle. Inlets to the tubes were chamfered to 45°. The flow coefficient for the nozzle (ratio of actual flow to ideal flow) was calculated to be approximately 0.8. The equivalent diameter of the mixer nozzle (diameter of a single tube with the same total exit area) was 3.98 centimeters with an area ratio, or ratio of the base area to the total flow area, of 8.2. The ratio of the side flow area between the tubes to the base area, or the ventilation factor, was about 1.5.

Instrumentation

The noise data were measured by fifteen 1.27-centimeter-diameter condenser microphones placed at various intervals on a 3.05-meter-radius circle around the nozzle/wing model, as shown in figure 6. The center of the microphone circle was at the exit of the 5.08-centimeter-diameter convergent nozzle. The microphone circle was in a horizontal plane 3.91 meters above an asphalt surface and perpendicular to the vertically mounted wing. The plane of the microphone circle passed through the nozzle axes. A standard piston calibrator (124±0.2 dB, 250-Hz tone) was used to calibrate the condenser microphones. Wind screens were placed on all microphones. The noise data were analyzed by a 1/3-octave-band spectrum analyzer.

Strain-gage pressure transducers were used to measure total pressures upstream of the nozzles. Temperatures were measured upstream of the nozzles by thermocouples immersed in the flow stream.

Weather data (barometer, temperature, humidity, and wind speed and direction) were also monitored and/or recorded.

Procedure

Far-field noise data were taken at various pressure ratios across the model nozzle and/or across the free-jet nozzle for a variety of conditions. The test configura-

tions and conditions are given in table I. These are summarized as follows: Each nozzle (conical or mixer) was tested both alone and with the wing (at flap positions of 10°-20°, 30°-60°, and 0°). For each configuration, data were obtained with only the free jet operating, with only the model jet operating, and with both the model and the free jet operating.

Typically, the test procedure was to obtain steady flow conditions for a given total pressure upstream of each nozzle. Three noise data samples were taken at each microphone location. An atmospheric loss correction was applied to the average of the three samples to give lossless sound pressure level data at a 3.05-meter radius. Ground reflections had an influence on the data below 200 hertz. Therefore, the spectral data were only considered from 200 hertz to 20 kilohertz.

It was found that the low-frequency noise (200 to 400 Hz) from the free jet contributed substantially to the total noise of the test configurations. Therefore, the free-jet noise was subtracted from the total test configuration noise. Thus, the effect of the external flow on the noise came from the small-scale model alone. The free-jet noise was obtained with the complete configuration in place but without flow through the test nozzles. In this manner, the free-jet noise spectra were determined at each of the free-jet test velocities. The subtraction of the free-jet noise was performed over the entire frequency range (200 Hz to 20 kHz). Above 500 hertz the separation between the two levels was so great in most cases that the correction was negligible. It was arbitrarily decided that, if the separation was less than 2 decibels, the data were unreliable and would be omitted from the analysis. The overall sound pressure levels were calculated from the corrected sound pressure levels at each microphone location.

Nozzle jet velocities were calculated from the isentropic equations by using the ratio of total to atmospheric pressures and the total temperature measured upstream of the nozzle exits.

AERODYNAMIC RESULTS

In references 3 and 5 it was demonstrated that flap noise for the static case (no external flow) could be correlated in terms of the sixth power of peak flap impingement velocity and the area of impingement. The peak velocities and the impingement areas were determined from velocity profiles that were obtained without the wing in place (nozzles alone). In this section it is shown how the velocity profiles (and hence impingement areas) and the peak velocities are influenced by external flow.

Velocity profiles downstream of the exits of the 5.08-centimeter-diameter conical nozzle and the eight-tube mixer nozzle were obtained as part of the study described in reference 6. In that study the nozzles were mounted in a 1.83-meter by 2.74-meter

wind tunnel that provided the external flow.

The effect of external flow on the velocity profiles for the conical and mixer nozzles alone is shown in figure 7. Data were taken at two axial locations downstream of the nozzle exits. Results from the conical nozzle (fig. 7(a)) show that the peak velocity is only slightly greater with external flow at a location close to the nozzle exit and near the end of the potential core (X/D = 5.15). Also, the width of the profile is greater with external flow; in the high-velocity region (e.g., at 80 percent of the peak velocity, or approx 240 m/sec) the profile with external flow is 17 percent wider than that without external flow. At a distance farther downstream of the nozzle exit (X/D = 13.4) the peak velocity with external flow is approximately 18 percent greater than that for the static condition; also, the profile is wider with external flow.

The mixer-nozzle profiles (fig. 7(b)) indicate that for both axial distances and/or external flow conditions the flow from the nozzle is still undeveloped, as shown by the radial displacement of the peak velocities. Farther downstream ($X/D_e > 9.6$) the flows from the individual jets coalesce and form a single parabolic profile, with the peak velocity occurring on the nozzle axis. At both axial locations shown in the figure the peak velocity is increased when the nozzle is subjected to external flow. However, the peak velocities are still well below the nozzle jet velocity of 315 meters per second. In contrast to the conical-nozzle results the profiles in the high-velocity region are slightly narrower with external flow.

Local peak velocity ratios as a function of X/D (or X/D_e for the mixer nozzle) are shown in figure 8. The conical- and mixer-nozzle data are from references 6 and 9, respectively. The results are typical for all nozzle jet velocities and show that a greater rate of velocity decay is obtained with the mixer nozzle. The effect of external flow occurs about 4 or 5 diameters (D_e for the mixer nozzle) downstream of the nozzle exits and influences the decay rate of the mixer nozzle more than that of the conical nozzle.

The 60° flap impingement location noted in figure 8 represents the distance along the nozzle axis from the nozzle exit to the impingement point on the trailing flap. Assuming a sixth-power relation between peak flap impingement velocity and jet-flap interaction noise (ref. 3), the increased velocity as a result of external flow would raise the jet-flap interaction sound levels of the conical-nozzle configuration by about 1 decibel. For the mixer nozzle, sound levels would be raised approximately 5 decibels, based solely on the increased flap impingement velocity. However, the results of reference 6 show that external flow attenuates jet mixing noise (possibly because of a reduction in shear at the jet boundary). Since noise sources in an EBF system include the jet noise and the jet-flap interaction noise, it is difficult to evaluate what the net effect would be. The following sections present the acoustic results for the EBF system used herein and show that the expected increase in the sound levels did not occur.

ACOUSTIC RESULTS

In this section, experimental data are presented to show the acoustic characteristics of the free jet and to establish the noise floor of the facility. This is followed by a comparison of the data for the nozzles alone (without the wing) with and without external flow. Corrections are made to the data for the nozzles alone in order to show the effects of convection and refraction that are caused both by the external flow and by the shear layer between the external flow field and the stationary ambient air. These corrections are made by the methods presented in references 10 and 11. The nozzle-alone data are then compared with other experiments in terms of the variation of the relative-velocity exponent with directivity angle.

The nozzle-plus-wing data are presented as measured, that is, corrections are not made for refraction and convection since the available theoretical methods are not believed to be directly applicable to this test configuration.

Free Jet

In figure 9, 1/3-octave-band spectra are presented for the free jet with the conical nozzle in place but with no flow. Data are presented for the conical nozzle alone and also for the conical nozzle/wing with various flap deflection angles. The data are shown for an angle of 90° from the nozzle inlet but are typical of the results for all angles from 40° to 100°. The sound levels for all configurations peak at 315 hertz and decrease rapidly above this frequency. The conical nozzle alone and the conical nozzle/wing with retracted flaps show similar trends from 315 hertz to about 6300 hertz. Similar agreement is also shown in the data for the nozzle/wing configurations with the flaps deflected to 10°-20° and 30°-60°. Above 6300 hertz the sound levels for all configurations decrease with about the same slope. The data in figure 9 show that the free jet operating alone (small nozzle inoperative) is primarily a low-frequency noise source regardless of the test model configuration.

One-third-octave-band spectra for the free jet with and without the conical nozzle operating (the wing is not in place in this configuration) are presented in figure 10. The data without the conical nozzle operating were taken from figure 9. Figure 10 illustrates the magnitudes of the differences in sound levels that occur when both nozzles are operating and when the free jet is operating alone. Also, the subtraction of the free-jet noise from the noise produced by both nozzles is illustrated.

For either flow condition (free jet plus conical nozzle or free jet alone) the free jet is acoustically dominant at 315 hertz and below (fig. 10). Above 315 hertz the noise from the conical nozzle becomes increasingly more dominant, as indicated by

the increase in separation of sound levels for the two flow conditions. The free-jet noise must be subtracted from the noise produced when both nozzles are operating in order to arrive at conditions that actually simulate the noise characteristics of the conical nozzle subjected to external flow. These data are shown in figure 10 as corrected data. For example, at 400 hertz the uncorrected sound pressure level is 77 decibels for flow from both nozzles (square symbols), whereas for flow from the large nozzle alone (free jet) the level is 73.5 decibels (circular symbols). The net result is a corrected level of 74.5 decibels for the conical nozzle with external flow (diamond symbols). As the difference between the noise produced by both nozzles and that produced by the free jet alone increases, the correction becomes smaller. At 800 hertz, for example, a difference of 15 decibels exists. With this magnitude, a correction of less than 0.2 decibel is subtracted from the noise produced by both nozzles to give the sound pressure level for the conical nozzle with external flow.

Test Nozzles without Wing

Conical-nozzle sound power level. - The variation of overall sound power level for the conical nozzle, without external flow, as a function of jet velocity is shown in figure 11. The data generally follow an eighth-power relation except for the highest value of jet velocity (340 m/sec). The deviation from the eighth-power relation in the high-velocity range is caused by the presence of shock noise. The sound power level spectra for various jet velocities and without external flow (fig. 12) suggest that the shock noise occurs at the high-frequency end of the spectra for the highest jet velocity tested (337 m/sec).

How external flow affects sound power level spectra at supersonic jet velocities (for fully expanded flow, the jet Mach number is 1.09) is shown in figure 13(a). External flow reduces the sound power level at the low-frequency end of the spectra (below 4000 Hz), but the levels are affected only slightly for frequencies above 8000 hertz. At subsonic jet velocities (fig. 13(b)) the sound power levels are reduced over the entire frequency range when the nozzle is subjected to external flow. This reduction in level is probably caused by a reduction in shear at the jet boundary that occurs when the nozzle flow is subjected to external flow.

Overall sound power level as a function of relative velocity (difference between nozzle jet velocity and external flow velocity, $V_j - V_f$) is shown in figure 14 for the conical nozzle alone. A family of curves is formed when the data are presented in this manner, implying that relative velocity alone does not correlate the data. At a given nozzle jet velocity, a reduction in sound power level occurs with an increase in external flow velocity. For subsonic nozzle jet velocities, a sixth-power relation with rela-

tive velocity is followed; for supersonic velocities, a fourth-power relation exists.

An analytical study presented in reference 12 suggests a subsonic jet noise reduction with forward velocity based on the relative velocity to the seventh power multiplied by the jet velocity. With this concept as a basis, all experimental data presented herein were correlated in terms of an external flow parameter that has the form

$$V_j\left(1 - \frac{V_f}{V_j}\right)^b$$

The exponent of the term in parentheses varied with the configuration and the directivity angle and was determined by curve fitting the experimental data.

The conical-nozzle overall sound power level data are shown in figure 15 as a function of the external flow parameter. The subsonic nozzle jet velocity data of figure 15 are adequately correlated by the form of the parameter shown. However, the supersonic data require a different form of the parameter and/or additional variables for correlation over the entire range of test conditions.

Conical-nozzle sound pressure level. - How external flow affects overall sound pressure level directivity patterns at supersonic velocities is shown in figure 16(a). External flow reduces the sound level over the entire acoustic field, with only minor changes in directivity. Sound pressure level spectra at 60° from the nozzle inlet are shown in figure 16(b) and reveal that broadband shock noise is present at the high-frequency end (above 4 kHz) of the spectra. Increasing external flow velocity, again, reduces the low-frequency sound level but has little effect on the sound level at the high-frequency end of the spectra for supersonic jet velocities. Comparing the 60° data with the sound pressure level at 90° (fig. 16(c)) shows that the peak level in the shock noise region is lower for the 90° data. At 160° from the nozzle inlet (fig. 16(d)) and with no external flow, the jet noise is dominant and completely masks the effect of shock noise. However, with external flow, remnants of the shock noise are evident at the high-frequency end (above 5 kHz) of the spectra. At this angle (160°) the low-frequency noise is considerably greater than at the other angles from the nozzle inlet, either with or without external flow.

Overall sound pressure level directivity patterns for a typical subsonic nozzle jet velocity are shown in figure 17(a). The levels are reduced as a result of external flow for all angles from the nozzle inlet. The spectra at 90° (fig. 17(b)) show a reduction in level over the entire frequency range when the test nozzle is subjected to external flow. The spectra at 160° (fig. 17(c)) show that the peak level at this angle occurs at the low-frequency end of the spectra, with a typical lowering of levels as a result of the influence of external flow.

To properly compare the static and dynamic data, it is desirable to have the same distance and angular position relative to the noise source for both cases. The data with external flow are influenced by convection and refraction caused by the external flow field since the microphones are placed outside the free stream. References 10 and 11 present an analytical method that can be used to correct for the refractive and convective effects in nozzle-alone tests. This analytical method was applied to the data shown in the directivity plots of figures 16(a) and 17(a), and the results are shown in figures 18(a) and (b), respectively. The figure indicates that the corrected sound levels, with external flow, are higher than the uncorrected levels in the forward quadrant ($\theta < 90^{\circ}$) and lower in the rearward quadrant. Also a change in directivity angle is apparent. The analysis is not applicable to angles greater than 150° in this instance, so the measured data at 155° and 160° were left uncorrected.

For the corrected sound pressure levels the data were plotted in terms of overall sound pressure level as a function of relative velocity ($V_j - V_f$) in order to determine the relative-velocity exponent. An example is shown in figure 19 for data at 90° from the nozzle inlet. For these data, no correction need be applied to the measured values. At a given subsonic nozzle jet velocity a 5.7-power relation exists, whereas for jet velocities above sonic a 4.2-power relation is shown. The exponents were determined from plots similar to the one shown in figure 20, where the change in overall sound pressure level is plotted as a function of jet velocity and relative velocity. The line drawn through the data was determined graphically, the slope being the relative-velocity exponent.

How the relative-velocity exponent, for the subsonic jet velocity data, varies as a function of directivity angle is shown in figure 21. The analyses of references 10 and 11 show that the corrected directivity angle is a function of free-stream Mach number, which explains the two sets of symbols in the figure.

The corrected relative-velocity exponent obtained from the tests described herein is compared with results from other experiments (refs. 13 to 15) in figure 22. The data are for conical nozzles with diameters ranging from 4.44 to 10.2 centimeters. Data from the references were obtained in acoustic wind tunnels; in reference 13 the microphones were outside the free stream, whereas in references 14 and 15 the microphones were within the flow from the wind tunnel. The area ratios are the ratios of free-stream area to nozzle exit area. The exponent generally increases with increasing directivity angle, and there is a considerable amount of scatter in the data from the various tests in the rearward quadrant ($\theta > 90^{\circ}$).

The overall sound pressure level at 90° for the conical nozzle without the wing is correlated with an external flow parameter in figure 23. Again, the supersonic data are displaced from the eighth-power curve faired through the subsonic data. When presented in this manner the product of the exponents ($8 \times 0.71 \approx 5.7$ in this case)

becomes the relative-velocity exponent shown in figure 22 as a function of directivity angle.

Mixer-nozzle sound power level. - Overall sound power level as a function of nozzle jet velocity for the eight-tube mixer nozzle alone, without external flow, is shown in figure 24. An eighth-power variation holds over the entire velocity range for this nozzle. The sound power level spectra (fig. 25) also show that the noise was generally broadband over the entire frequency range. For this nozzle, the shock noise at the highest velocity was beyond the range of these data (frequency >20 kHz) because of the small tube diameters. Increasing the diameter of the individual tubes would lower the frequency at which the shock noise occurs. For example, in acoustic tests for a six-tube mixer nozzle with individual tube diameters of 2.36 centimeters (ref. 16), shock noise was present at approximately 20 kilohertz for a jet velocity of 337 meters per second.

How external flow affects the sound power level spectra for the mixer nozzle is shown in figure 26. The results are generally similar to those for the conical nozzle in that the levels are reduced over the entire frequency range when the nozzle is subjected to external flow.

The variation of overall sound power level with relative velocity is shown in figure 27. For a given jet velocity the sound power is proportional to the sixth power of relative velocity. The overall sound power level is correlated with an external flow parameter in figure 28; the correlation is similar to that for the conical nozzle.

Mixer-nozzle sound pressure level. - Overall sound pressure level directivity patterns at 3.05 meters for the eight-tube mixer nozzle alone are shown in figure 29(a) for a subsonic nozzle jet velocity and various external flow velocities. The results are typical of all nozzle jet velocities tested. Sound levels are reduced at all angles because of external flow, and the patterns are generally similar except in the rearward quadrants near the nozzle axis (e.g., 140° to 160° from nozzle inlet). The spectra for three different angular locations are shown in figures 29(b) to (d). Sound pressure levels are reduced over the entire frequency range at all angles when the nozzle is subjected to external flow, with the greatest reduction occurring at 160° (fig. 29(d)).

The overall sound pressure level data shown in figure 29(a) were corrected for refraction and convection and compared with the measured data (fig. 30). Again, as with the conical nozzle, the levels for the corrected data are greater in the forward quadrant ($\theta < 90^{\circ}$) and less in the rearward quadrant. Relative-velocity exponents for the mixer nozzle were determined from the corrected data in the same manner as was used for the conical nozzle (see fig. 20) and plotted as a function of directivity angle in figure 31. At a given angle the exponent for the mixer nozzle is less than that found for the conical nozzle (compare with fig. 21).

The overall sound pressure level at 90° as a function of the external flow parame-

ter is shown in figure 32, where again the product of the exponents ($8 \times 0.61 \approx 4.9$) is the relative-velocity exponent shown in figure 31.

Test Nozzles with Wing

Conical nozzle. - The overall sound pressure level directivity patterns at 3.05 meters for the conical nozzle/wing, for typical simulated landing conditions, are shown in figure 33(a). The wing flaps were set at 30°-60°, and the nozzle jet velocity was 208 meters per second. Data for two values of external flow are shown, as well as for the static case. Maximum external flow velocity with the wing in place was limited to about 54 meters per second in order to avoid structural damage to the wing model. Only a slight reduction in sound levels occurred when the model was subjected to external flow, except at 150° from the nozzle inlet. Directivity, in general, was also unaffected by external flow. The spectra at 80° from the nozzle inlet (fig. 33(b)), or the peak flyover noise location, show only a slight reduction in levels over the entire frequency range, with the largest effect occurring in the low-frequency region (315 to 1250 Hz). Nozzle-alone data are included in the figure for comparison. Similar results are reported in reference 17 for large-scale-model wind tunnel tests. The results presented in figure 33 are typical for other values of nozzle jet velocity and other angles.

The overall sound pressure level at 80° as a function of relative velocity for the 30°-60° flap setting configuration are shown in figure 34. The data in the figure indicate a 1.17-power relation for a given jet velocity and imply a relative insensitivity to external flow effects for this configuration. The overall sound pressure level at 80° is correlated with an external flow parameter in figure 35. A seventh-power relation applies over the entire range of test conditions. Examination of the spectra at this angle for the supersonic jet velocity data both for the conical nozzle alone and for the nozzle with wing (fig. 36) leads to the following observations: The shock noise for the nozzle alone (at approx 10 kHz) is considerably less than the flap noise (low-frequency region), and does not contribute substantially to the overall noise level for the nozzle-wing configuration.

The relation among the overall sound pressure level at various angles, the relative velocity, and the external flow parameter is summarized in table II. The table shows the relation for the 5.08-centimeter-diameter conical nozzle/wing with various flap deflection angles. The data for the 10°-20° and retracted flap settings are discussed in subsequent sections. The equations accompanying the table show that overall sound pressure level, at a given angle, is proportional to either the relative velocity raised to a power a or to the velocity parameter raised to a power c. The exponent b of

the term in parentheses varied with the angle from the nozzle inlet and/or with the configuration tested and is also listed in the table. All exponents (a, b, c) were determined by curve fitting the data.

Normalized sound pressure level as a function of Strouhal number is shown in figure 37 for the conical nozzle/wing with the 30°-60° flap setting. The data are for an angle of 80° from the nozzle inlet. Sound pressure levels for each spectrum are normalized by subtracting the overall sound pressure level from the sound pressure level at a given 1/3-octave-band center frequency. The supersonic jet velocity (336 m/sec) data were not used in this correlation since it was felt that the spectra were influenced by the shock noise (even though the overall level was not appreciably affected by the shock noise). The Strouhal number was based on the diameter of the conical nozzle (5.08 cm) and on the nozzle jet velocity V_j. The data in figure 37(a) show a relatively broad band characteristic with a peak occurring at a Strouhal number of about 0.6. For Strouhal numbers above 0.2 the data are correlated satisfactorily. Below this value, however, the data scatter increases. By removing the data for the static case (no external flow), a better agreement over the entire range of test conditions was obtained when correlated with either jet velocity (fig. 37(b)) or relative velocity (fig. 37(c)). Similar results, in terms of spectral shape and peak Strouhal number, were obtained for other angles from the nozzle inlet.

Typical noise radiation patterns for a takeoff flap setting of 10°-20°, with the conical nozzle, are shown in figure 38(a). Greater attenuation occurred for this flap setting than occurred for the 30°-60° setting (fig. 33(a)) when the wing model was exposed to external flow. Directivities were generally the same for either the static case or the case with external flow. The spectra at 100° (fig. 38(b)), or near the peak flyover noise location, indicate an attenuation over the entire frequency range as a result of external flow. Data for the nozzle without the wing are included for comparative purposes.

The overall sound pressure level at 100° as a function of relative velocity (fig. 39) shows a 3.3-power relation for a given nozzle jet velocity. In the correlation of the overall level at 100° with the external flow parameter (fig. 40), the supersonic data (V_j of 340 m/sec) are displaced from the seventh-power curve faired through the subsonic data points. Comparing the spectra for the nozzle alone and for the nozzle/wing with 10°-20° flaps for the supersonic velocity data (fig. 41) shows that nozzle shock noise is dominant at the high-frequency end of the spectra and influences the overall levels enough for the 10°-20° configuration to cause the discrepancy evident in figure 40.

Comparing the data for the takeoff configuration (10°-20° flap setting) with the wind tunnel results presented in reference 15 shows similar trends, in that attenuation occurs as a result of external flow. However, the absolute values of attenuation are

not in agreement, which could be attributed to the differences in model configurations for the two experiments.

Normalized sound pressure level spectra at 100° from the nozzle inlet for the 10°-20° flap setting are shown in figure 42. The data peak at a Strouhal number of about 0.3 and, as with the 30°-60° flap data, show an increased amount of scatter for the lower Strouhal numbers but good agreement for the higher numbers.

The noise data for the conical nozzle/wing with the flaps in the retracted setting are presented in figure 43. The overall sound pressure level (fig. 43(a)) shows that an even greater attenuation occurs, as a result of external flow, for this flap setting than occurs for the two other configurations (30°-60°, 10°-20°). The spectra directly under the wing (fig. 43(b)) and at the maximum flyover noise location (fig. 43(c)) show that attenuation occurs at all frequencies. The overall sound pressure level at 120° follows a 6.5-power relation with relative velocity (fig. 44) and correlates with the seventh power of the external flow parameter (fig. 45).

Summarizing, the general trend is to show increasing amounts of attenuation as a result of external flow as the wing flaps are progressively retracted from the airstream. The absolute values of the sound levels are, of course, lower when the flaps are raised.

Mixer nozzle. - The increase in velocity at the flap impingement location when the mixer nozzle is subjected to external flow (fig. 8(b)) implies an increase of about 5 decibels in flap noise as a result of the dependence of flap noise on the sixth power of flap impingement velocity. However, except for differences in levels caused by differences in nozzle type and size, the results obtained with the mixer nozzle were generally similar to those obtained with the conical nozzle. That is, sound levels were reduced and directivity patterns were not altered when the mixer-nozzle/wing combination was exposed to external flow.

The noise data for the mixer nozzle/wing with the 30°-60° flap setting are shown in figure 46. The overall sound pressure level at 3.05 meters (fig. 46(a)) shows that external flow causes only a slight noise reduction for this configuration at angles from 40° to 100°. The spectra at 80° from the nozzle inlet (fig. 46(b)) show that external flow reduces the noise levels in the low- and high-frequency ranges with little or no attenuation of the middle frequencies.

The overall sound pressure level at 80° for the 30°-60° flap setting as a function of relative velocity is shown in figure 47. At a given nozzle jet velocity the sound varies as the 1.6 power of relative velocity. Correlating the overall level at 80° (fig. 48) shows that the level at this angle varies as the seventh power of the external flow parameter.

Normalized sound pressure level spectra for the mixer nozzle/wing with the 30°-60° flap setting (fig. 49) show scattering trends that are similar to those for the

conical nozzle (fig. 37(a)). For example, for high Strouhal numbers, the data correlated fairly well; for low Strouhal numbers, however, the data scatter increased. The Strouhal number in figure 49 is based on the equivalent diameter of the mixer nozzle (3.98 cm).

Table III summarizes the functional relations between the overall sound pressure level at various angles and the relative velocity and external flow parameter for the mixer nozzle/wing with various flap settings. The trends are generally similar to those found for the conical nozzle. That is, increasing amounts of attenuation were obtained, as a result of external flow, as the wing flaps were raised.

Flap impingement velocity. - As reported in references 3 to 5, flap noise without external flow can be correlated in terms of the sixth power of peak flap impingement velocity. Peak-velocity decay rates for the mixer nozzle, similar to those shown in figure 8, were obtained as part of the experimental work reported in reference 6. In that work, data were obtained over a range of jet velocities and external flows so that local peak velocities at the flap impingement station, measured along the nozzle axis, could be calculated for the test conditions reported herein. In figure 50(a) the overall sound pressure level at 80° from the nozzle inlet is shown for the mixer nozzle/wing with the 30°-60° flap setting as a function of the peak flap impingement velocity. The data show that at a given nozzle exhaust velocity the overall sound pressure level decreases when the flap impingement velocity is increased by increasing external flow. Figure 50(b) shows the results for the 10°-20° flap setting at 100° from the nozzle inlet. The reduction in level is greater than for the 30° 60° setting for a given change in impingement velocity.

The data for the 30°-60° flap setting at 80° from the nozzle inlet are correlated in figure 51(a) in terms of the peak flap impingement velocity without external flow $\left(V_{ip}\right)_0$ and a multiplying factor similar to that used to correlate the data with the jet velocity (fig. 48). The overall sound pressure level follows a sixth-power relation when correlated in this manner. For zero external flow velocity the results agree with those reported in references 3 to 5.

The correlation of overall sound pressure level at 100° from the nozzle inlet for a flap setting of 10°-20° is shown in figure 51(b). The multiplier of $\left(V_{ip}\right)_0$ for this configuration is also similar to the one employed to correlate the data with the jet velocity (table III). Results of the correlation of overall sound pressure level at various angles from the nozzle inlet with the peak flap impingement velocity are listed in table IV for the 30°-60° and 10°-20° flap settings.

Symmetrical airfoil with mixer nozzle. - As part of the work reported in reference 18, the mixer nozzle used herein was tested with a symmetrical airfoil having its chord line placed parallel to the nozzle axis. Therefore, the angle of attack of the

wing with respect to the nozzle axis was zero. Consequently, the trailing edge of the airfoil was moved farther away from the high-velocity flow field of the mixer nozzle (fig. 7(b)). For example, for the nozzle/wing configuration with the flaps retracted, the trailing edge of the wing was 6.5 centimeters ($r/D_e = 1.6$) above the nozzle axis. However, for the symmetrical airfoil with its chord line parallel to the nozzle axis (fig. 5(a)), this distance increased to 9.15 centimeters ($r/D_e = 2.3$). An examination of figure 7(b) illustrates the approximate reduction in the velocity at the trailing edge with this increase in distance.

The overall sound pressure level radiation patterns for this configuration change are compared in figure 52(a). The effect on the directivity patterns is relatively minor either with or without external flow. The greatest disagreement in spectral distribution occurred at 120° from the nozzle inlet. These data are compared in figure 52(b) and show that there is a 2- to 3-decibel separation in the high-frequency region of the spectra either with or without external flow. At other directivity angles the differences were minor and/or inconsistent in trends.

A sample of the spectral data at 90° for the symmetrical airfoil is shown in figure 53 for different jet velocities. Greater attenuation occurs, as a result of external flow, in the high-frequency region of the spectra for the lowest jet velocity tested.

SOURCE-MOTION EFFECTS

The presentation of the nozzle/wing model results thus far has been for a stationary noise source as well as for a stationary observer. In a situation where the noise source is moving relative to the observer, such as an airplane flyover, other effects must be taken into consideration. These are the convective amplification of the noise and the Doppler shift in frequency.

In estimating the source-motion effect on the model results, the flap noise is assumed to be radiating from a point dipole on the trailing flap, and the work of reference 19 is applied to the data reported herein. Reference 19 gives the relative-motion effect for a point-dipole noise source. The convective amplification is given by

$$\Delta(\mathrm{OASPL})_D = (\mathrm{OASPL})_{\mathrm{flight}} - (\mathrm{OASPL})_{\mathrm{static}} = -40 \log \left[1 - \left(\frac{V_f}{c_0} \right) \cos \theta \right] \qquad (1)$$

and the effect on frequency by

$$f_D = \frac{f}{\left[1 - \left(\frac{V_f}{c_0}\right)\cos\theta\right]} \tag{2}$$

The attenuation due to external flow can be obtained from the functional relations of table II (conical nozzle). The change in overall sound pressure level is given by

$$\Delta(\text{OASPL})_f = (\text{OASPL})_{\text{flight}} - (\text{OASPL})_{\text{static}} = 10bc \log\left(\frac{V_j - V_f}{V_j}\right) \tag{3}$$

The product of the exponents bc is a function of the trailing-flap setting and the angle from the nozzle inlet. The net effect on overall sound pressure level for a moving source can be written as

$$(\text{OASPL})_{\text{net}} = (\text{OASPL})_{\text{static}} - 40 \log\left[1 - \left(\frac{V_f}{c_0}\right)\cos\theta\right] + 10bc \log\left(\frac{V_j - V_f}{V_j}\right) \tag{4}$$

An example of the overall sound pressure level radiation patterns that show the calculated effect of source motion is given in figure 54. An ambient speed of sound c_0 of 335 meters per second was used for the evaluation of equation (1). In figure 54(a), data for a trailing-flap setting of 60° are given and show that the net overall sound pressure level for angles close to the nozzle inlet is higher than that for the stationary source with external flow. For angles greater than 90°, more attenuation occurs as a result of these effects. For the 20° flap setting (fig. 54(b)) the trends are similar.

SUMMARY OF RESULTS

The results of an investigation of the effect of simulated forward velocity (generated by a free jet) on the acoustic characteristics of a model of an under-the-wing, externally blown flap (EBF) lift augmentation system with a conical nozzle and an eight-tube mixer nozzle can be summarized as follows:

1. Simulated forward velocity (approx 54 m/sec) attenuates the noise from an EBF system. The degree of attenuation depends on the trailing-flap settings and the directivity angle, with less attenuation occurring at the higher flap settings. With the 60° trailing-flap setting the OASPL at a directivity angle of 90° is reduced by about 1 decibel; with the 20° flap setting the OASPL at the same directivity angle is reduced by 4 decibels.

2. Noise radiation patterns for the EBF model were unchanged, over the range of

conditions investigated, when the model was subjected to simulated forward velocity.

3. The calculated effect of source motion shows that with either the 20° or 60° trailing-flap setting the noise level in the forward quadrant (0° to 90°) under the wing is greater than that measured with a stationary source subjected to simulated forward velocity. However, the calculations show that a lower noise level than was measured with the stationary source occurs in the rearward quadrant ($>90^{\circ}$) as a result of source motion.

4. For the conical nozzle/wing with the 60° trailing-flap setting the relative-velocity exponent varied with directivity angle, ranging from 1.17 to 2.4. With the 20° flap setting the exponent was almost invariant, ranging from 3.3 to 3.8.

For the mixer nozzle/wing with the 60° flap setting the exponent increased continuously from 0.27 at 40° from the nozzle inlet to 3.1 at 100°. With the 20° flap setting the exponent ranged from 3.9 to 5.4.

5. The effect of simulated forward velocity on the conical nozzle/wing with the 60° flap setting was to reduce the low-frequency sound levels (200 to 1600 Hz). The high-frequency sound levels (above 2000 Hz) in the forward quadrant and under the wing were generally unaffected by simulated velocity. With the 20° flap setting the sound levels were reduced over the entire frequency range.

For the mixer nozzle/wing with the 60° flap setting the low-frequency (200 to 630 Hz) and high-frequency (5 to 20 kHz) sound levels were reduced as a result of simulated forward velocity. The middle frequency range (800 Hz to 4 kHz) was unaffected. With the 20° flap setting the sound levels were reduced over the entire frequency range.

6. Overall sound power level for the conical nozzle alone varied as the sixth power of relative velocity for subsonic jet velocities. For supersonic jet velocities the variation was a fourth-power relation. The supersonic jet velocity data showed a double-peak power spectra with or without simulated forward velocity. The high-frequency peak sound power level (8000 Hz) was caused by shock noise and was unaffected when the model was subjected to forward velocities; the low-frequency peak sound power level (1250 Hz) was attenuated.

7. Overall sound power levels for the mixer nozzle alone varied as the sixth power of relative velocity over the entire range of conditions tested.

Lewis Research Center,
National Aeronautics and Space Administration,
Cleveland, Ohio, April 30, 1976,
505-05.

APPENDIX - SYMBOLS

a, b, c	constants used in tables I, II, and III
c_0	ambient speed of sound, m/sec
D	diameter, cm
D_e	equivalent diameter, $\sqrt{4(\text{Total area})/\pi}$, cm
f	emitted frequency, Hz
f_D	observed frequency caused by Doppler effect, Hz
$(\text{OASPL})_{net}$	overall sound pressure level defined by eq. (4), dB referenced to 2×10^{-5} N/m^2
$(\text{OASPL})_{static}$	measured overall sound pressure level without external flow, dB referenced to 2×10^{-5} N/m^2
$\Delta(\text{OASPL})_D$	change in overall sound pressure level caused by convective amplification
$\Delta(\text{OASPL})_f$	change in overall sound pressure level caused by external flow, dB
r	radial distance from nozzle axis, cm
V	local peak velocity, m/sec
ΔV	relative velocity, $V_j - V_f$, m/sec
V_f	external flow velocity (free jet), m/sec
V_{ip}	peak flap impingement velocity, m/sec
$(V_{ip})_0$	peak flap impingement velocity without external flow, m/sec
V_j	jet velocity, m/sec
X	distance downstream of nozzle exit, cm
X_i	distance downstream of nozzle exit to impingement point on 60° flap measured along nozzle axis, cm
θ	angle from nozzle inlet, deg

REFERENCES

1. Dorsch, R. G.; Kreim, W. J.; and Olsen, W. A.: Externally-Blown-Flap Noise. AIAA Paper 72-129, Jan. 1972.

2. Olsen, William A.; Dorsch, Robert G.; and Miles, Jeffrey H.: Noise Produced by a Small-Scale, Externally Blown Flap. NASA TN D-6636, 1972.

3. Dorsch, R. G.; Goodykoontz, J. H.; and Sargent, N. B.: Effect of Configuration Variation on Externally Blown Flap Noise. AIAA Paper 74-190, Jan. 1974.

4. Goodykoontz, Jack H.; Wagner, Jack M.; and Sargent, Noel B.: Noise Measurements for Various Configurations of a Model of a Mixer-Nozzle Externally Blown Flap System. NASA TM X-2776, 1973.

5. Goodykoontz, J. H.; Dorsch, R. G.; and Wagner, J. M.: Acoustic Characteristics of Externally Blown Flap Systems with Mixer Nozzles. AIAA Paper 74-192, Jan. 1974.

6. von Glahn, U. H.; Groesbeck, D. E.; and Goodykoontz, J. H.: Velocity Decay and Acoustic Characteristics of Various Nozzle Geometries with Forward Velocity. AIAA Paper 73-629, July 1973.

7. Parlett, Lysle P.; Freeman, Delma C., Jr.; and Smith, Charles C., Jr.: Wind-Tunnel Investigation of a Jet Transport Airplane Configuration with High Thrust-Weight Ratio and an External-Flow Jet Flap. NASA TN D-6058, 1970.

8. Freeman, Delma C., Jr.; Parlett, Lysle P.; and Henderson, Robert L.: Wind-Tunnel Investigation of a Jet Transport Airplane Configuration with an External-Flow Jet Flap and Inboard Pod-Mounted Engines. NASA TN D-7004, 1970.

9. Dorsch, Robert G.; and Reshotko, Meyer: EBF Noise Tests with Engine Under-the-Wing and Over-the-Wing Configurations. STOL Technology. NASA SP-320, 1972, pp. 455-473.

10. Amiet, R. K.: Correction of Open Jet Wind Tunnel Measurements for Shear Layer Refraction. AIAA Paper 75-532, Mar. 1975.

11. Amiet, R. K.: Frame of Reference Considerations for the Forward Flight Noise Problem. Rept. N212775-1, United Aircraft Res. Labs., 1974.

12. Ffowcs Williams, J. E.: The Noise from Turbulence Convected at High Speed. Phil. Trans. Royal Soc. (London), ser. A, vol. 255, no. 1061, Apr. 18, 1963, pp. 469-503.

13. de Belleral, J. F.; Chen, C. Y.; and Perulli, M.: Investigation of In-Flight Jet Noise Based on Measurements in an Anechoic Wind Tunnel. T. P. No. 1975-80, Office National D'Etude Et de Recherches Aerospatiales (France), 1975.

14. Cocking, B. J.; and Bryce, W. D.: Subsonic Jet Noise in Flight Based on Some Recent Wind-Tunnel Tests. AIAA Paper 75-462, Mar. 1975.

15. Pennock, A. P.; Swift, G.; and Marbert, J. A.: Static and Wind Tunnel Model Tests for the Development of Externally Blown Flap Noise Reduction Techniques. (LG74ER0170, Lockheed-Georgia Co.; NAS3-16831) NASA CR-134675, 1975.

16. von Glahn, U.; and Goodykoontz, J.: Installation and Air Speed Effects on Jet-Shock-Associated Noise. NASA TM X-71792, 1975.

17. Falarski, Michael D.; Aoyagi, Kiyoshi; and Koenig, David G.: Acoustic Characteristics of Large-Scale STOL Models at Forward Speed. STOL Technology. NASA SP-320, pp. 443-454.

18. von Glahn, U.; Goodykoontz, J.; and Wagner, J.: Nozzle Geometry and Forward Velocity Effects on Noise for CTOL Engine-Over-the-Wing Concept. NASA TM X-71453, 1973.

19. Lighthill, M. J.: Sound Generated Aerodynamically. Proc. Roy. Soc. (London), vol. 267A, no. 1329, May 1962, pp. 147-182.

TABLE I. - TEST CONFIGURATIONS AND CONDITIONS

Test nozzle	Wing configuration	Flow condition			
		Model jet		Free jet	
		On	Off	On	Off
Conical nozzle	No wing	×			×
			×	×	
		×		×	
	10^{o}-20^{o} Flaps	×			×
			×	×	
		×		×	
	30^{o}-60^{o} Flaps	×			×
			×	×	
		×		×	
	Retracted flaps	×			×
			×	×	
		×		×	
Mixer nozzle	No wing	×			×
			×	×	
		×		×	
	10^{o}-20^{o} Flaps	×			×
			×	×	
		×		×	
	30^{o}-60^{o} Flaps	×			×
			×	×	
		×		×	
	Retracted flaps	×			×
			×	×	
		×		×	

TABLE II. - RELATION AMONG OVERALL SOUND PRESSURE LEVEL AT VARIOUS ANGLES, RELATIVE VELOCITY, AND EXTERNAL FLOW PARAMETER FOR THE CONICAL NOZZLE/WING WITH VARIOUS FLAP SETTINGS

$$\left[\mathrm{OASPL} \propto (V_j - V_f)^a;\ \mathrm{OASPL} \propto \left[V_j\left(1 - \frac{V_f}{V_j}\right)^b\right]^c\right].$$

Wing configuration	Angle from nozzle inlet, θ, deg	Constant		
		a	b	c
30^{o}-60^{o} Flaps	40	1.95	0.325	6
	60	1.35	.225	6
	80	1.17	.167	7
	90	2.1	.263	8
	100	2.4	.267	9
10^{o}-20^{o} Flaps	40	3.8	0.633	6
	60	3.5	.583	↓
	80	3.4	.567	↓
	90	3.4	.567	↓
	100	3.3	.471	7
	120	3.3	.471	7
Retracted flaps	40	4.4	0.628	7
	60	6.0	1.0	6
	80	6.3	1.05	6
	90	6.0	1.0	6
	100	6.1	.87	7
	120	6.5	.93	7
	140	6.9	.86	8

TABLE III. - RELATION AMONG OVERALL SOUND PRESSURE LEVEL AT VARIOUS ANGLES, RELATIVE VELOCITY, AND EXTERNAL FLOW PARAMETER FOR THE MIXER NOZZLE/WING WITH VARIOUS FLAP SETTINGS

$$\left[\mathrm{OASPL} \propto (V_j - V_f)^a;\ \mathrm{OASPL} \propto \left[V_j\left(1 - \frac{V_f}{V_j}\right)^b\right]^c\right].$$

Wing configuration	Angle from nozzle inlet, θ, deg	Constant		
		a	b	c
30^o-60^o Flaps	40	0.27	0.038	7
	60	.865	.123	↓
	80	1.6	.228	↓
	90	2.15	.307	↓
	100	3.1	.387	8
10^o-20^o Flaps	40	3.9	0.557	7
	60	5.2	.743	↓
	80	5.4	.771	↓
	90	5.1	.728	↓
	100	4.71	.673	↓
	120	4.56	.651	↓
	140	4.54	.567	8
Retracted flaps	40	3.14	0.392	8
	60	5.6	.70	8
	80	6.2	.775	8
	100	5.7	.814	7
	120	5.1	.637	8
	140	5.2	.650	8

TABLE IV. - FUNCTIONAL RELATION BETWEEN OVERALL SOUND PRESSURE LEVEL AND PEAK FLAP IMPINGEMENT VELOCITY FOR THE MIXER NOZZLE/WING WITH VARIOUS FLAP SETTINGS

$$\left[\mathrm{OASPL} \propto \left[\left(V_{ip}\right)_0\left(1 - \frac{V_f}{V_j}\right)^b\right]^c\right].$$

Wing configuration	Angle from nozzle inlet, θ, deg	Constant	
		b	c
30^o-60^o Flaps	40	0.05	6
	60	.10	↓
	80	.20	↓
	90	.20	↓
	100	.25	↓
10^o-20^o Flaps	40	0.60	6
	60	.75	↓
	80	↓	↓
	90	↓	↓
	100	↓	↓
	120	↓	↓
	140	↓	7

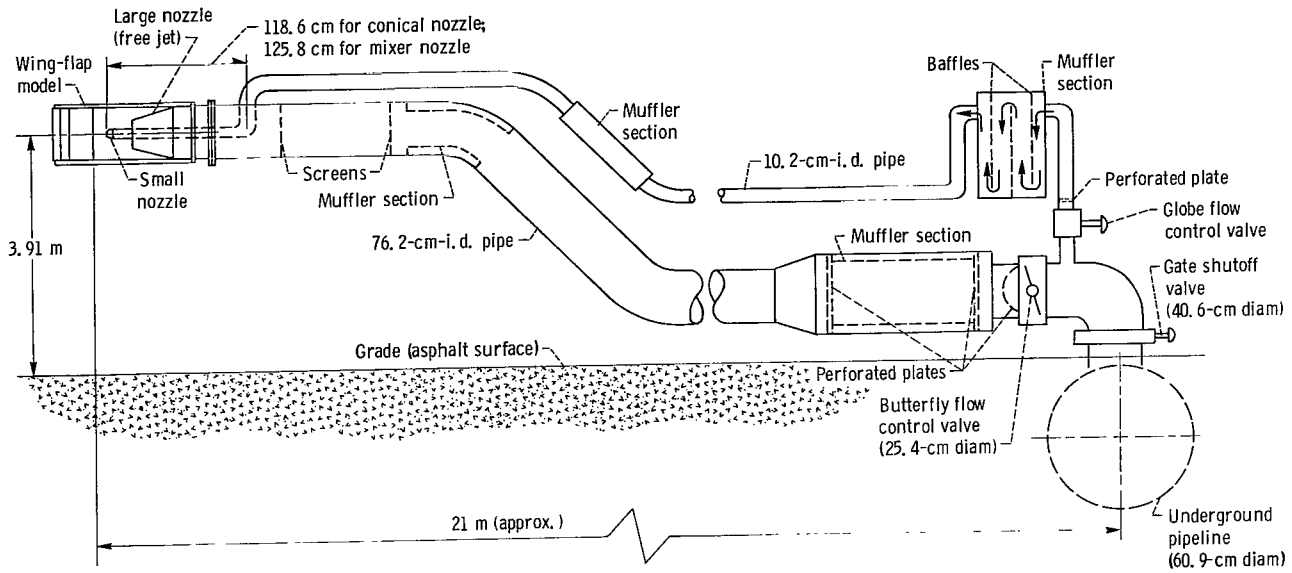

Figure 1. - Airflow system.

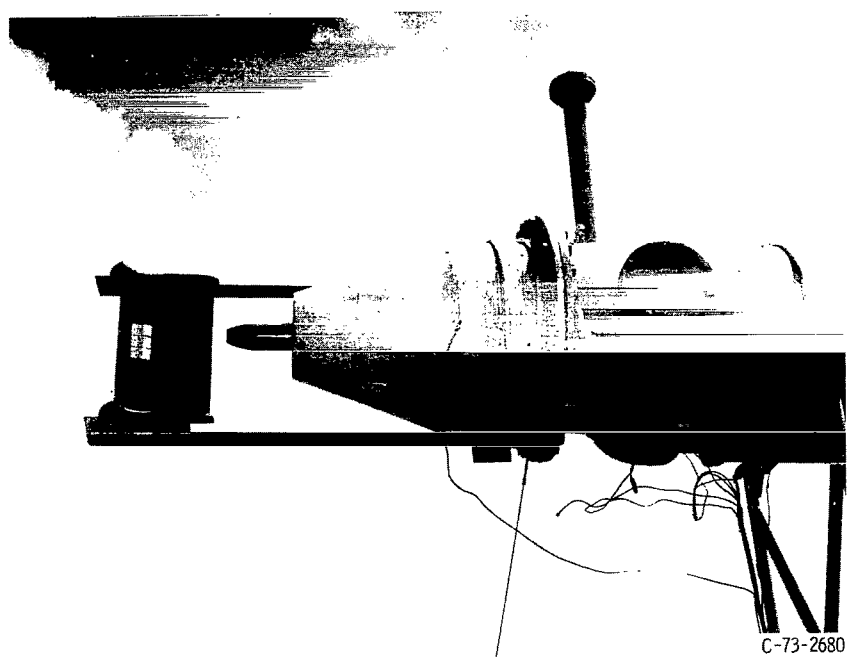

Figure 2. - Test installation with 5.08-centimeter-diameter conical nozzle and wing.

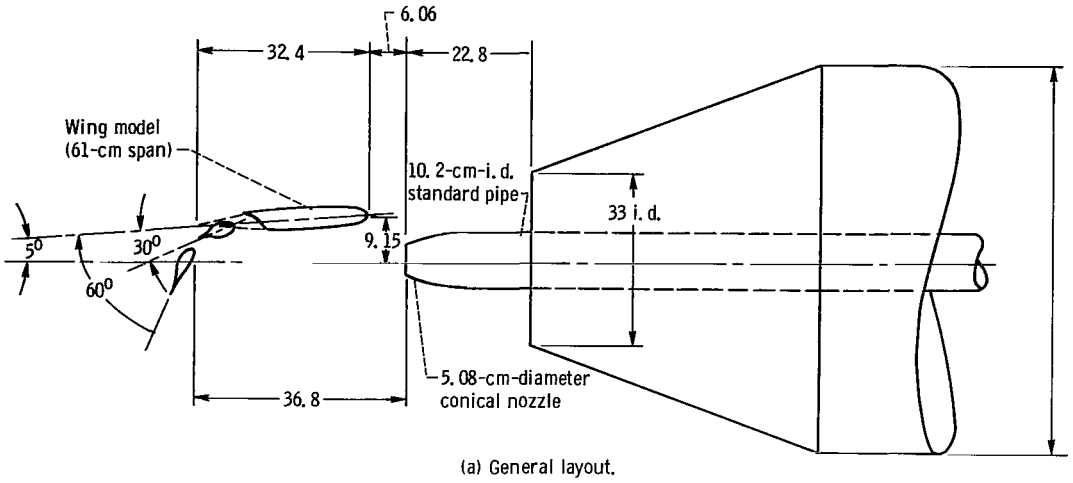

(a) General layout.

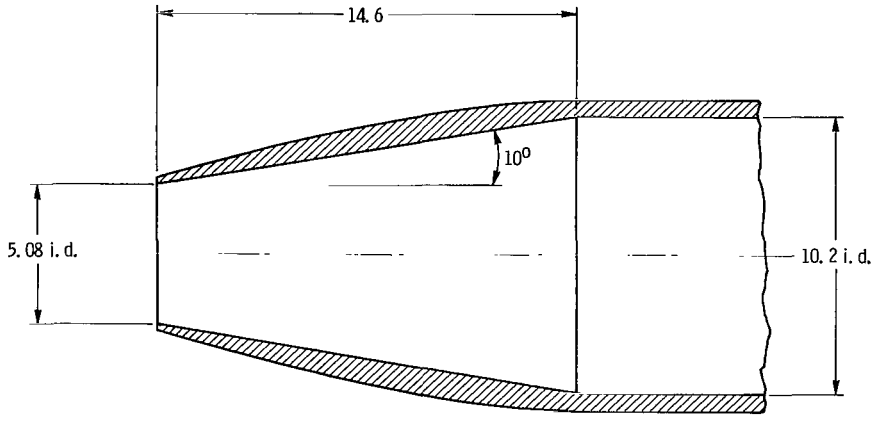

(b) Conical nozzle detail.

Figure 3. - Model dimensions and configuration for 5.08-centimeter-diameter conical nozzle installation. Wing flaps in landing setting (30^{0}-60^{0}). (All dimensions in centimeters.)

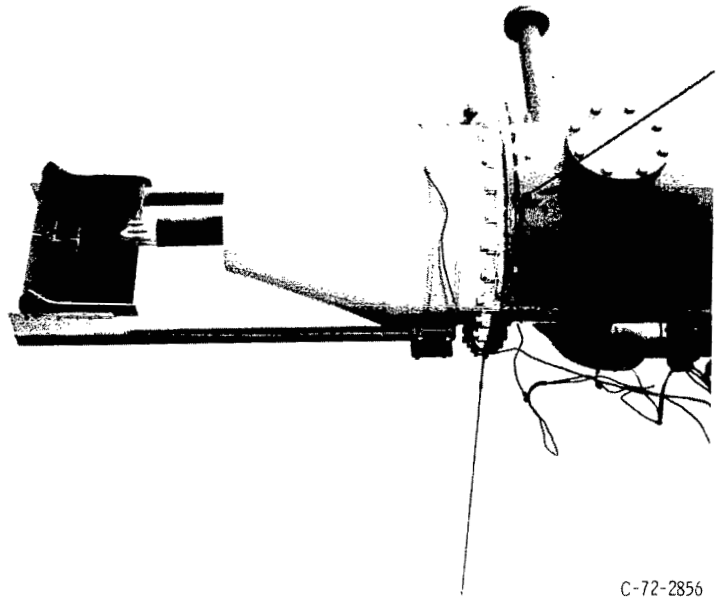

C-72-2856

Figure 4. - Test installation with eight-tube mixer nozzle and wing.

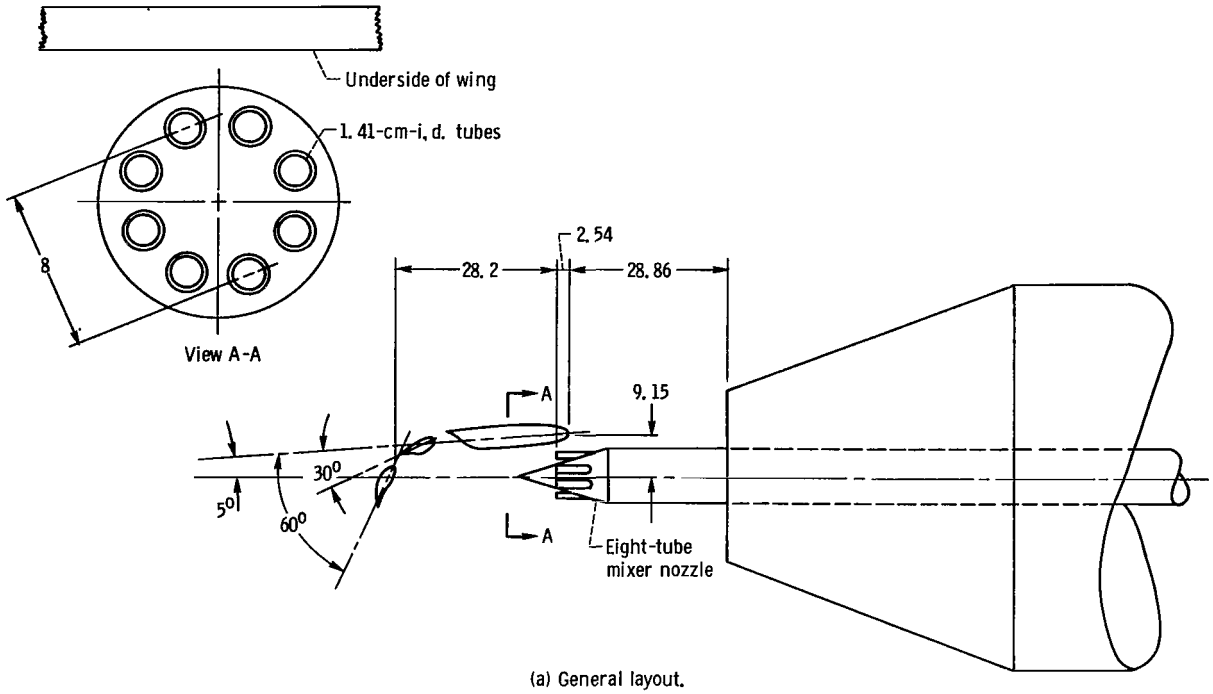

(a) General layout.

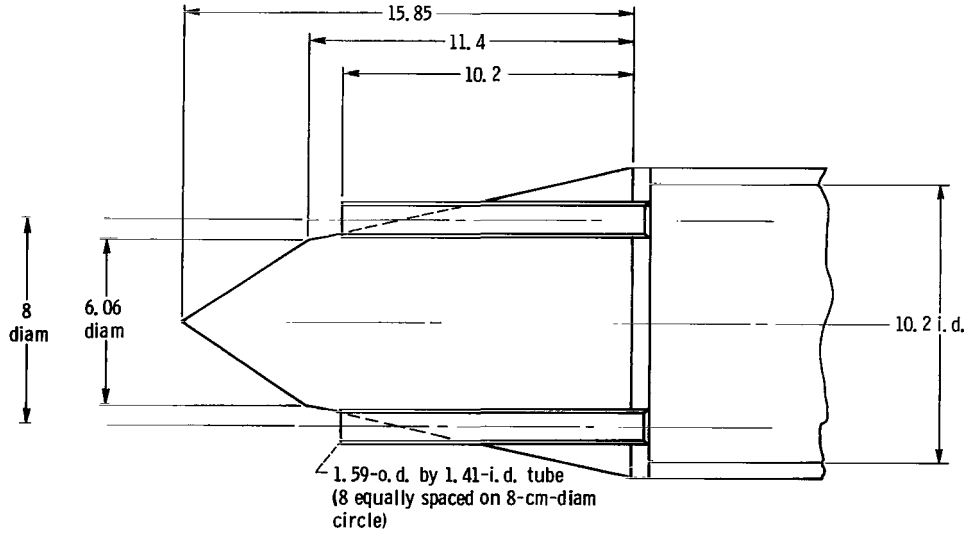

(b) Eight-tube mixer nozzle detail; equivalent diameter, D_e, 3.98 centimeters.

Figure 5. - Model dimensions and configuration for eight-tube mixer nozzle installation. Wing flaps in landing setting (30^0-60^0). (All dimensions in centimeters.)

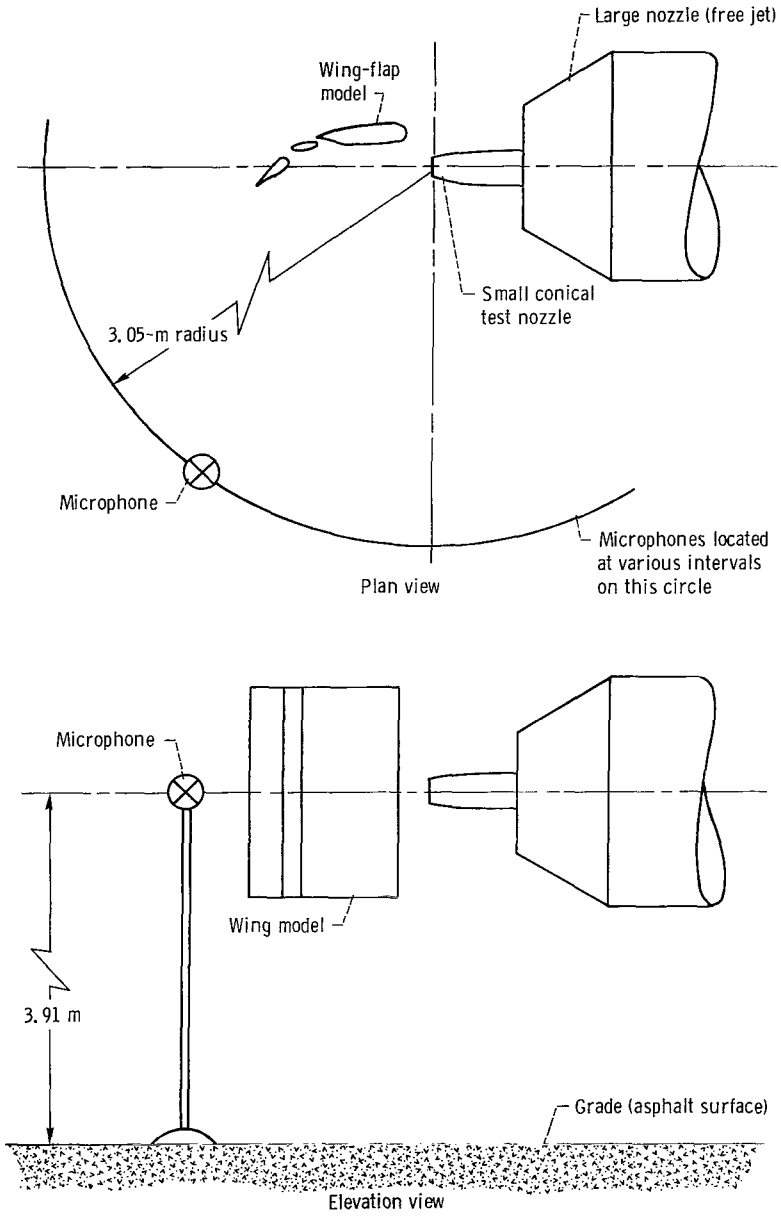

Figure 6. - Microphone placement.

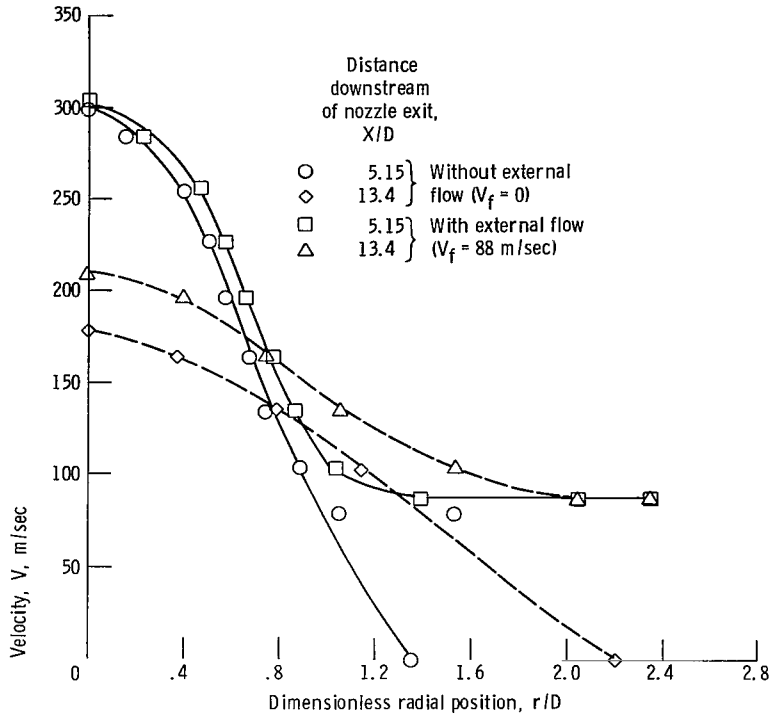

(a) Conical nozzle; nozzle jet velocity, V_j, 306 meters per second.

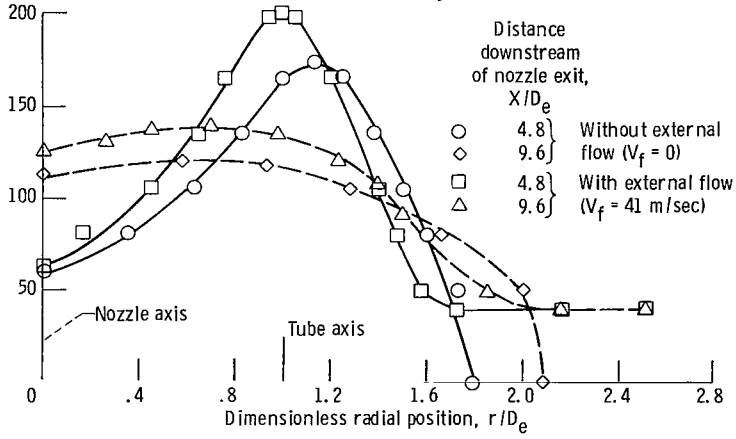

(b) Eight-tube mixer nozzle; nozzle velocity, V_j, 315 meters per second.

Figure 7. - Velocity profiles for model nozzles alone with and without external flow at two different distances downstream of nozzle exit. (Wind tunnel data from ref. 6.)

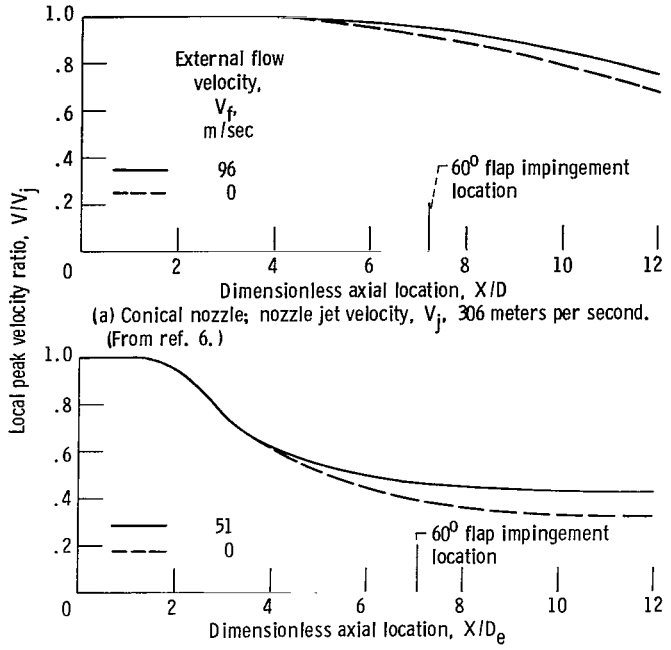

(a) Conical nozzle; nozzle jet velocity, V_j, 306 meters per second. (From ref. 6.)

(b) Eight-tube mixer nozzle; nozzle jet velocity, V_j, 254 meters per second. (From ref. 9.)

Figure 8. - Local peak velocity decay for conical and eight-tube mixer nozzles both with and without external flow.

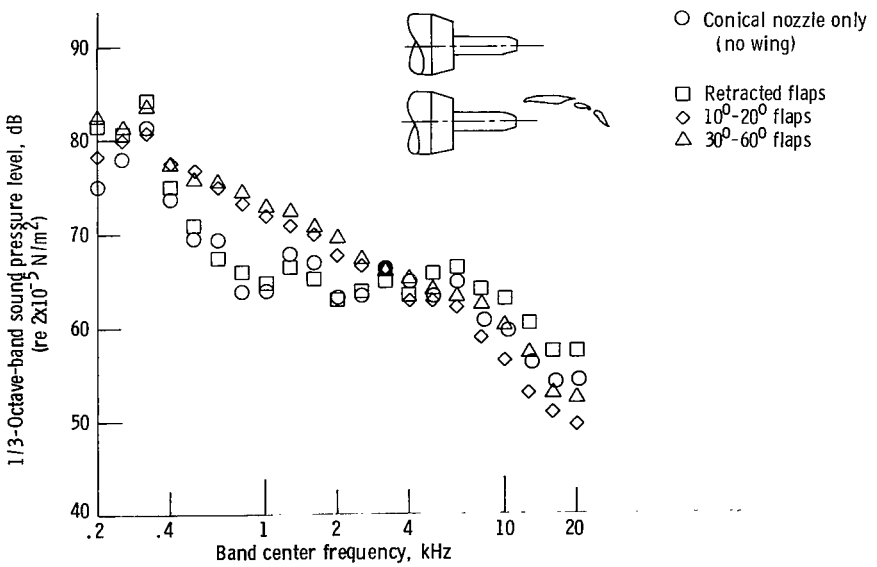

Figure 9. - Comparison of spectra for various small model configurations and flow from free jet only. Microphone distance, 3.05 meters; angle from nozzle inlet, θ, 90^0; external flow velocity, V_f, 53 meters per second; nozzle jet velocity, V_j, 0.

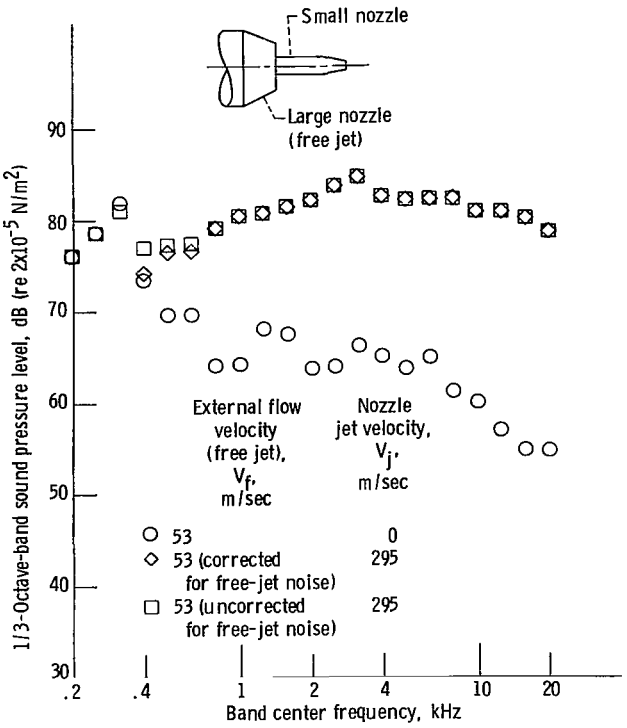

Figure 10. - Comparison of spectra for the free jet with and without 5.08-centimeter-diameter conical nozzle operating. Microphone distance, 3.05 meters; angle from nozzle inlet, θ, 90^0.

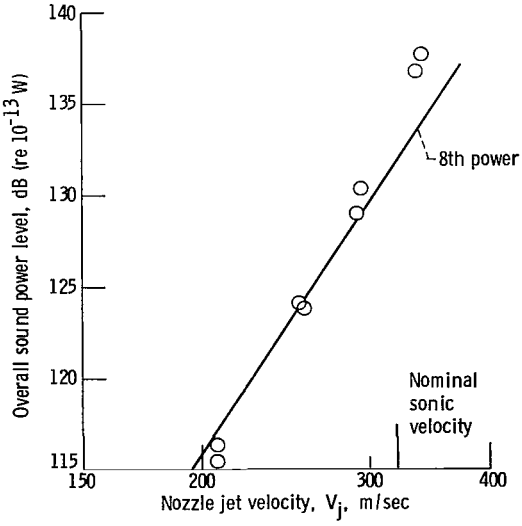

Figure 11. - Overall sound power level as function of nozzle jet velocity for 5.08-centimeter-diameter convergent nozzle alone without external flow.

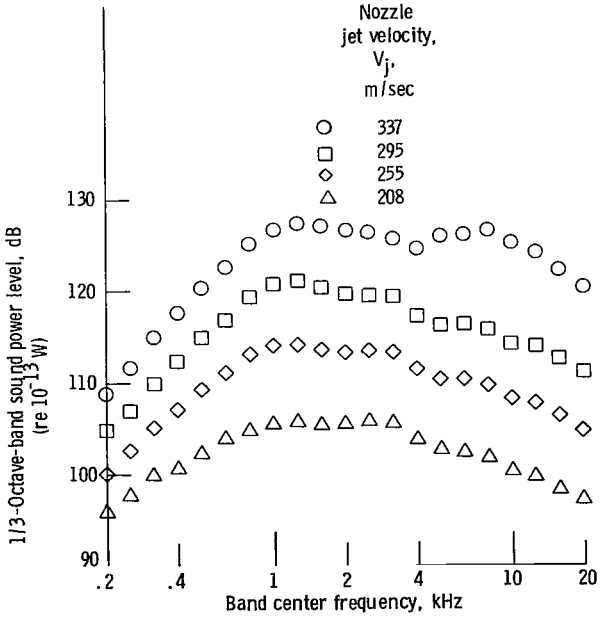

Figure 12. - Sound power level spectra for 5.08-centimeter-diameter conical nozzle alone without external flow.

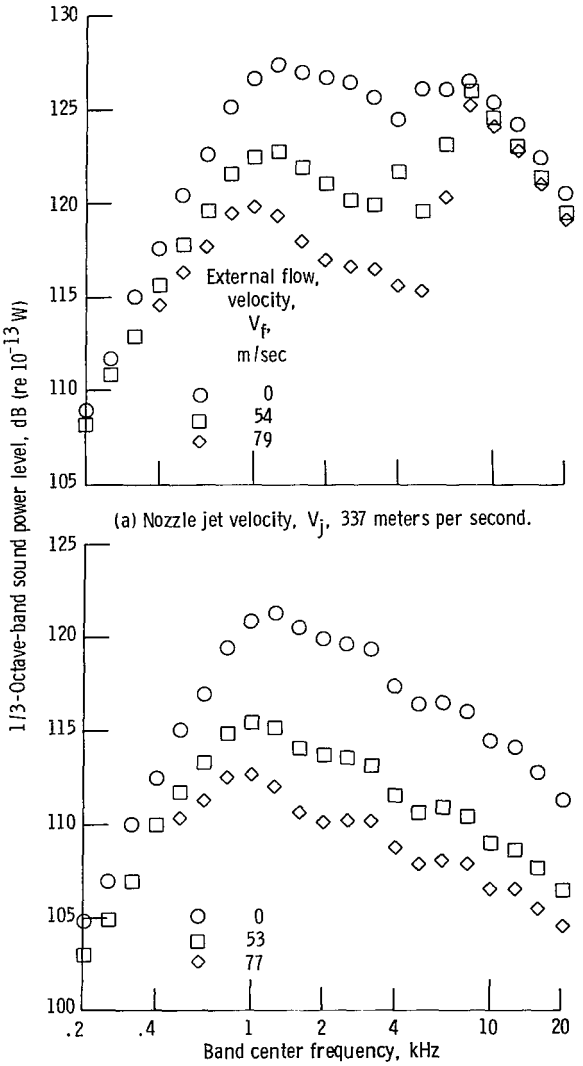

(a) Nozzle jet velocity, V_j, 337 meters per second.

(b) Nozzle jet velocity, V_j, 295 meters per second.

Figure 13. - Sound power level spectra for 5.08-centimeter-diameter nozzle alone with external flow.

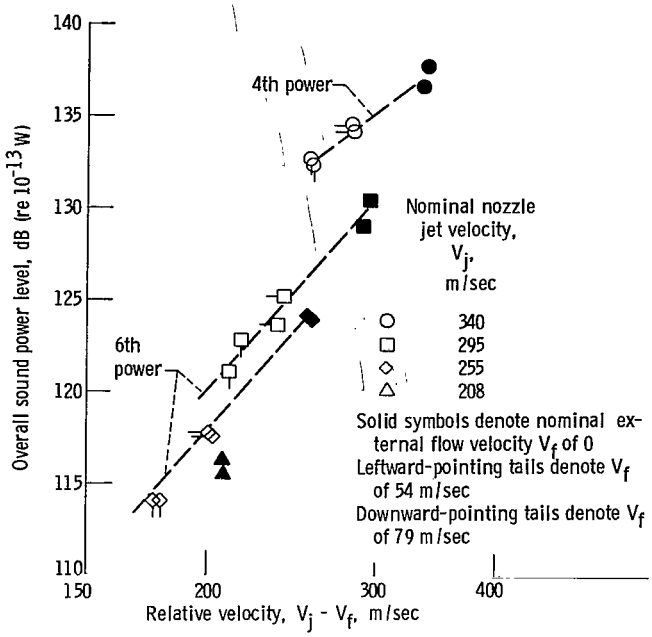

Figure 14. - Overall sound power level as function of relative velocity for 5.08-centimeter-diameter conical nozzle alone.

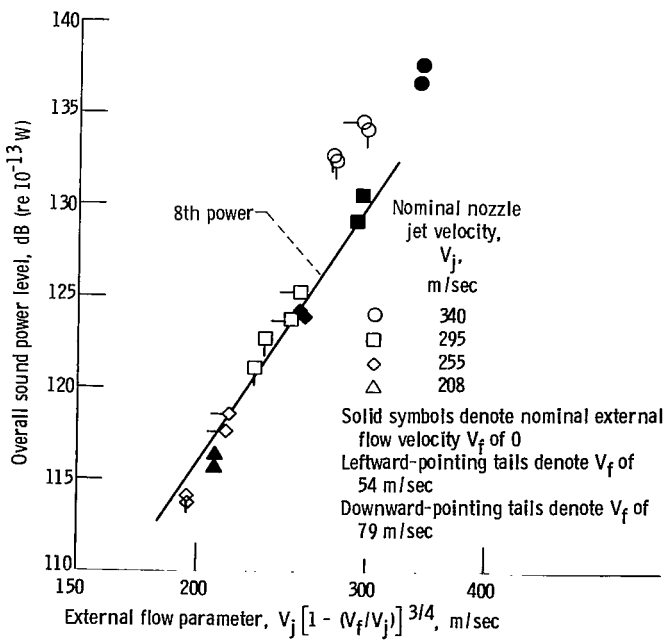

Figure 15. - Overall sound power level as function of external flow parameter for 5.08-centimeter-diameter conical nozzle alone.

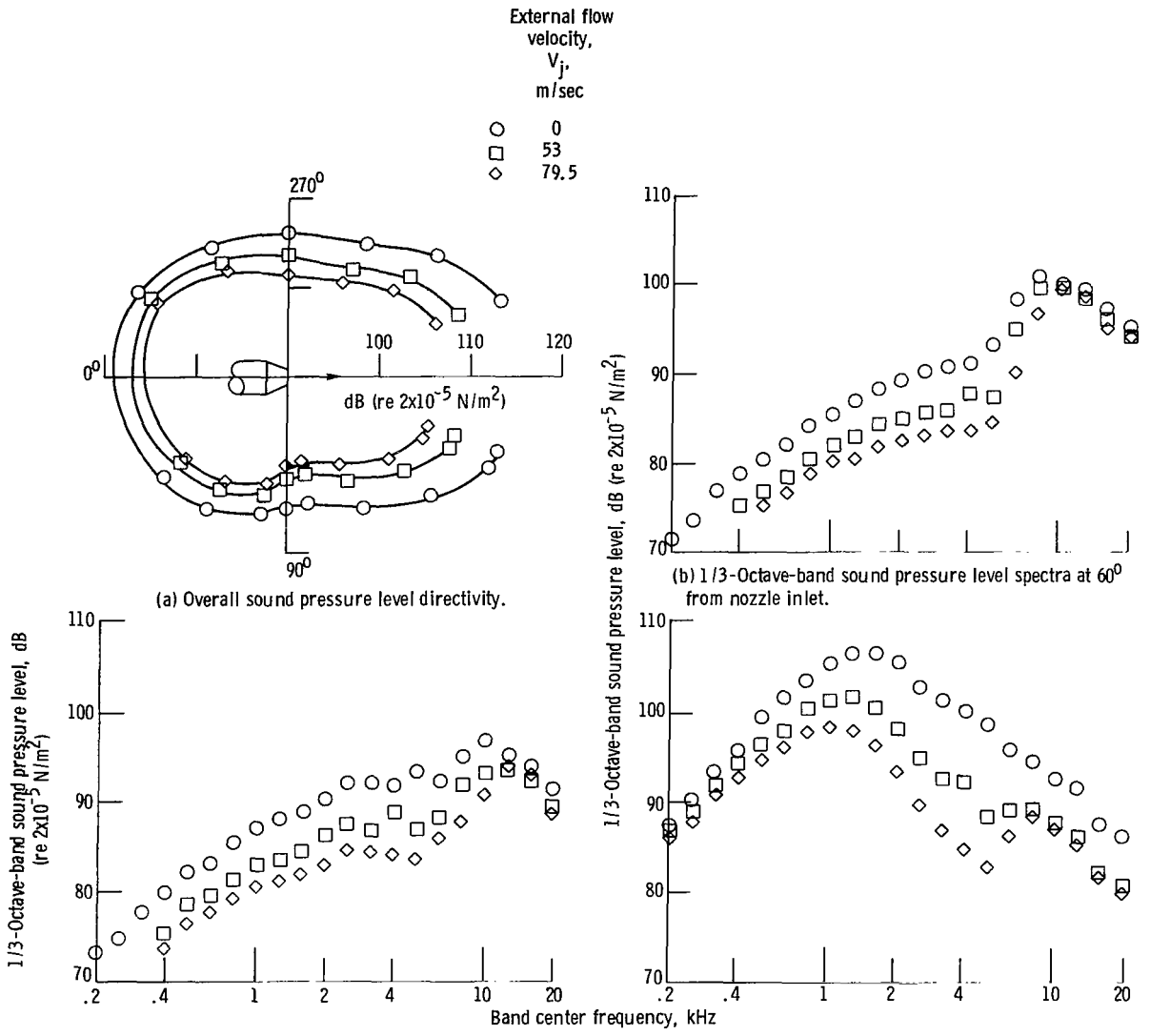

(a) Overall sound pressure level directivity.

(b) 1/3-Octave-band sound pressure level spectra at 60° from nozzle inlet.

(c) 1/3-Octave-band sound pressure level spectra at 90° from nozzle inlet.

(d) 1/3-Octave-band sound pressure level spectra at 160° from nozzle inlet.

Figure 16. - Effect of external flow on sound levels from the 5.08-centimeter-diameter conical nozzle alone. Nozzle jet velocity, V_j, 337 meters per second; microphone distance, 3.05 meters.

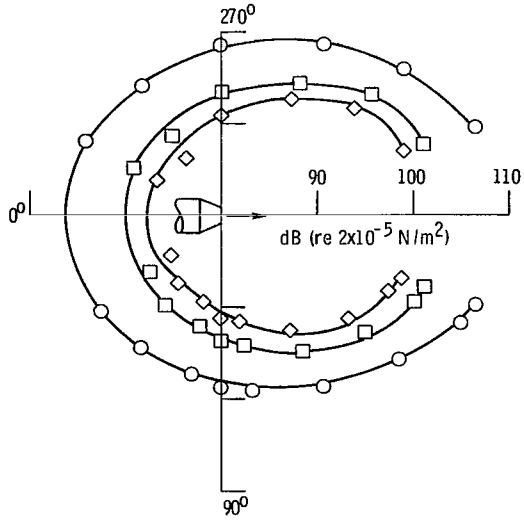

(a) Overall sound pressure level directivity.

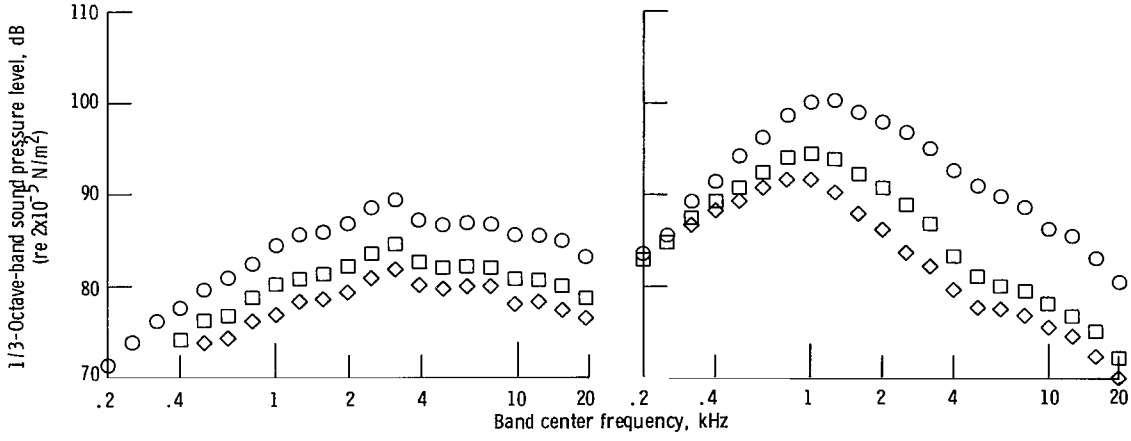

(b) 1/3-Octave-band sound pressure level spectra at 90° from nozzle inlet.

(c) 1/3-Octave-band sound pressure level spectra at 160° from nozzle inlet.

Figure 17. - Effect of external flow on sound levels from 5.08-centimeter-diameter nozzle alone. Nozzle jet velocity, V_j, 295 meters per second; microphone distance, 3.05 meters.

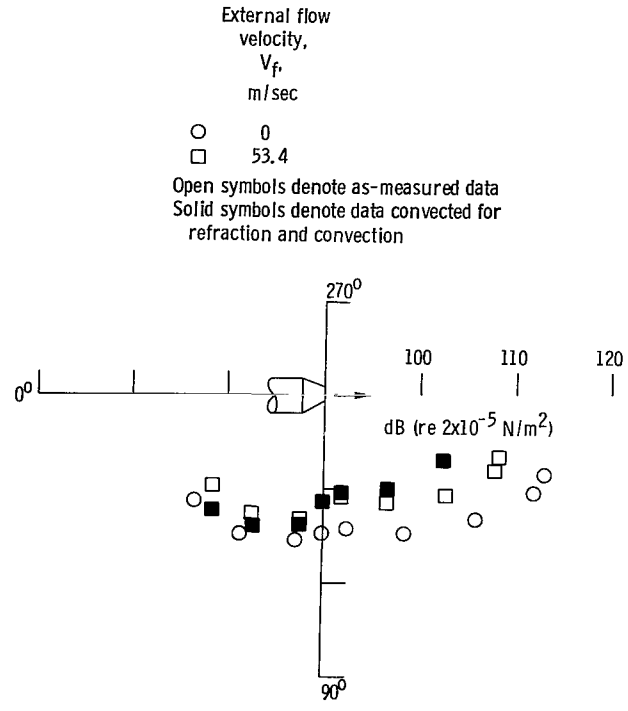

(a) Nozzle jet velocity, V_j, 337 meters per second.

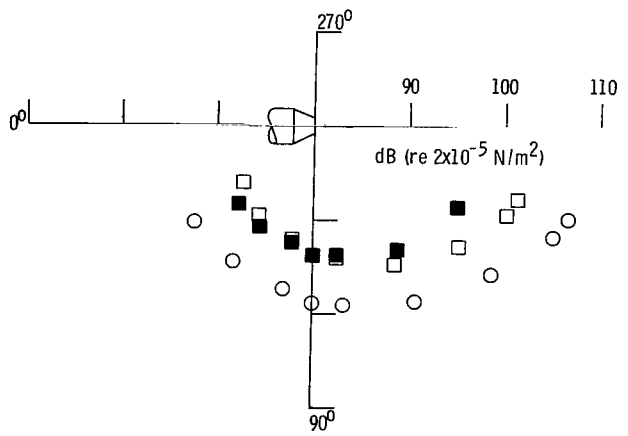

(b) Nozzle jet velocity, V_j, 295 meters per second.

Figure 18. - Comparison of sound levels with and without corrections for refraction and convection, for conical nozzle alone. Microphone distance, 3.05 meters.

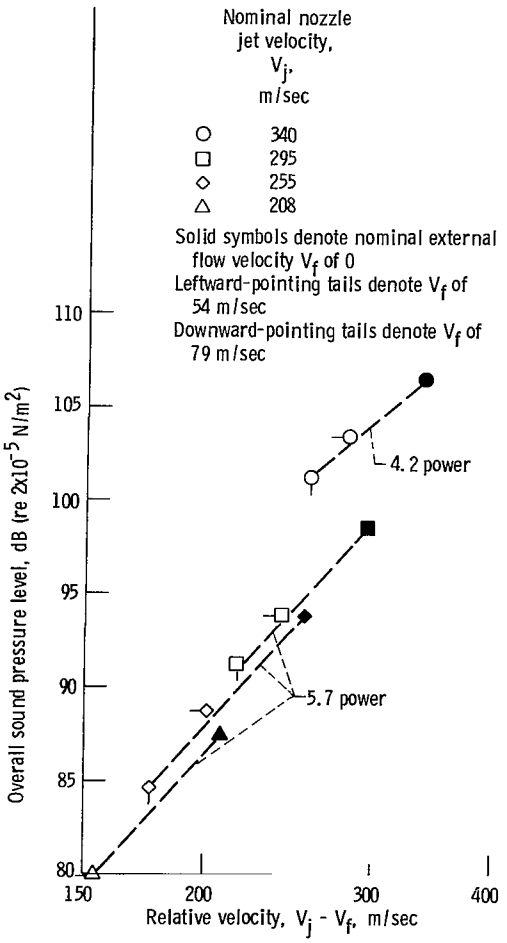

Figure 19. - Overall sound pressure level at 90° from nozzle inlet as function of relative velocity for conical nozzle alone. Microphone distance, 3.05 meters.

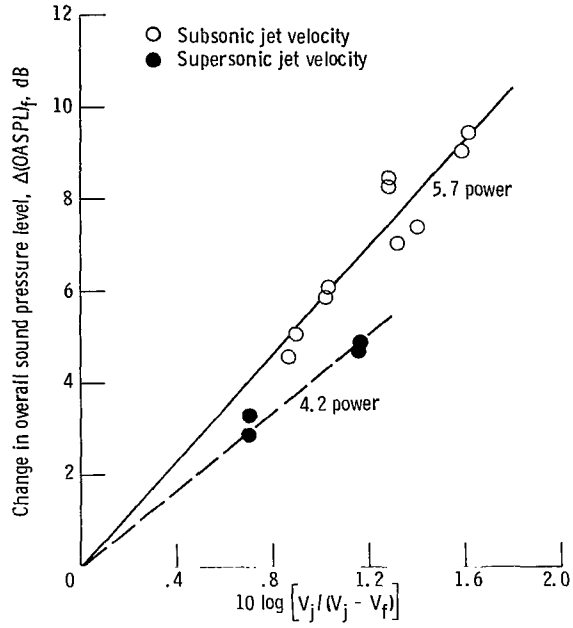

Figure 20. - Changes in overall sound pressure level caused by external flow as function of jet velocity and relative velocity. Slope of curves is relative velocity exponent. Angle from nozzle inlet, θ, 90°.

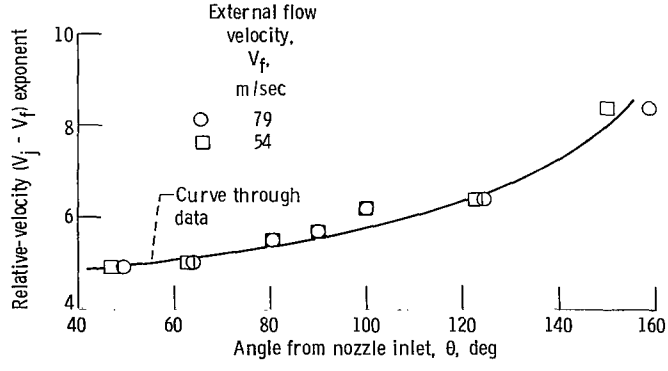

Figure 21. - Relative-velocity exponent as function of directivity angle for conical nozzle alone. Data corrected for refraction and convection.

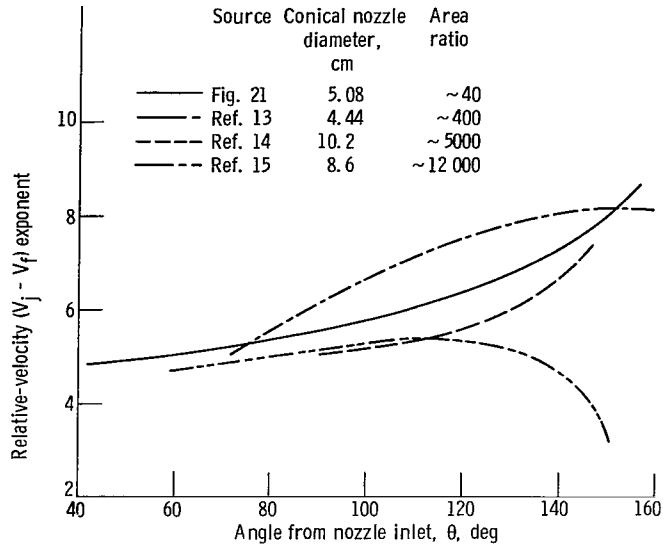

Figure 22. - Comparison of relative-velocity exponents for conical nozzles alone from various experiments.

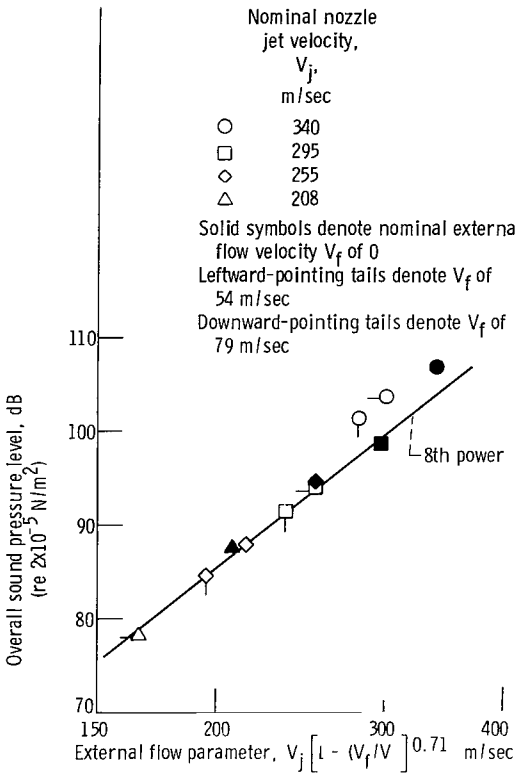

Figure 23. - Overall sound pressure level at 90° from nozzle inlet as function of an external flow parameter for conical nozzle alone. Microphone radius, 3.05 meters.

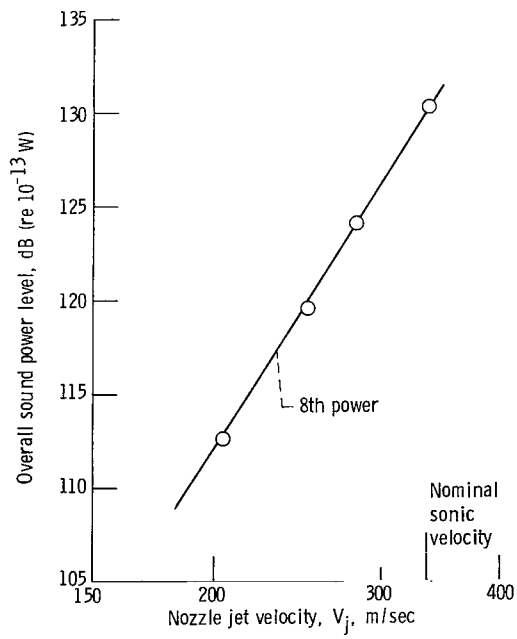

Figure 24. - Overall sound power level as function of nozzle jet velocity for eight-tube mixer nozzle alone without external flow

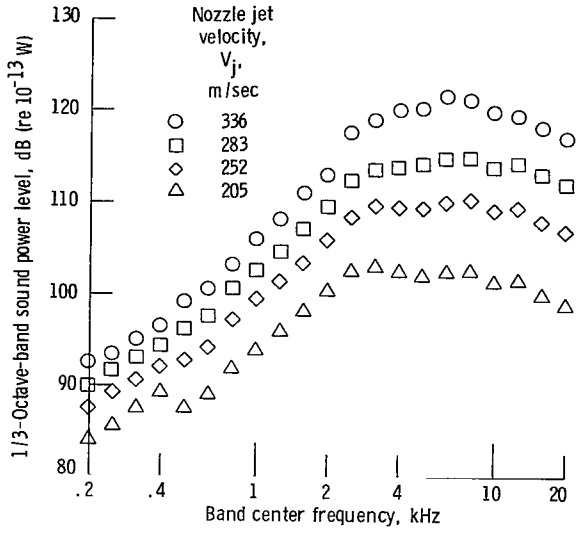

Figure 25. - Sound power level spectra for eight-tube mixer nozzle alone without external flow.

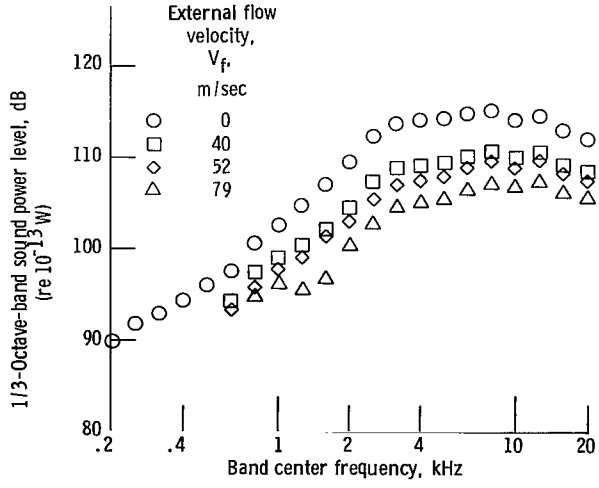

Figure 26. - Sound power level spectra as function of external flow for eight-tube mixer nozzle alone. Nozzle jet velocity, V_j, 283 meters per second.

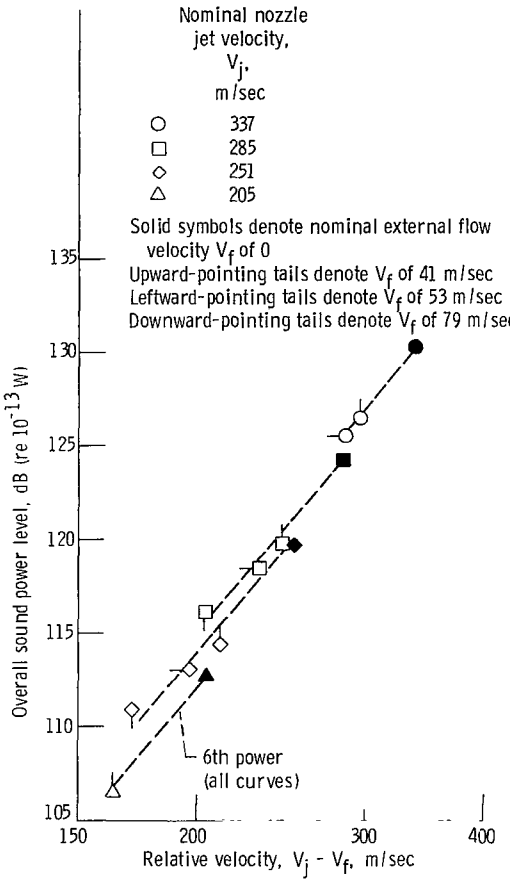

Figure 27. - Overall sound power level as function of relative velocity for eight-tube mixer nozzle alone.

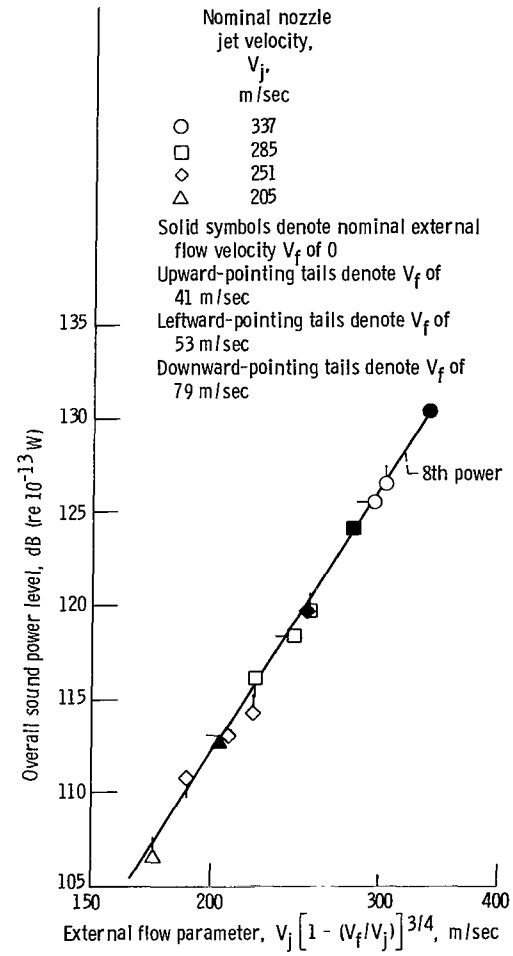

Figure 28. - Overall sound power level as function of an external flow parameter for eight-tube mixer nozzle alone.

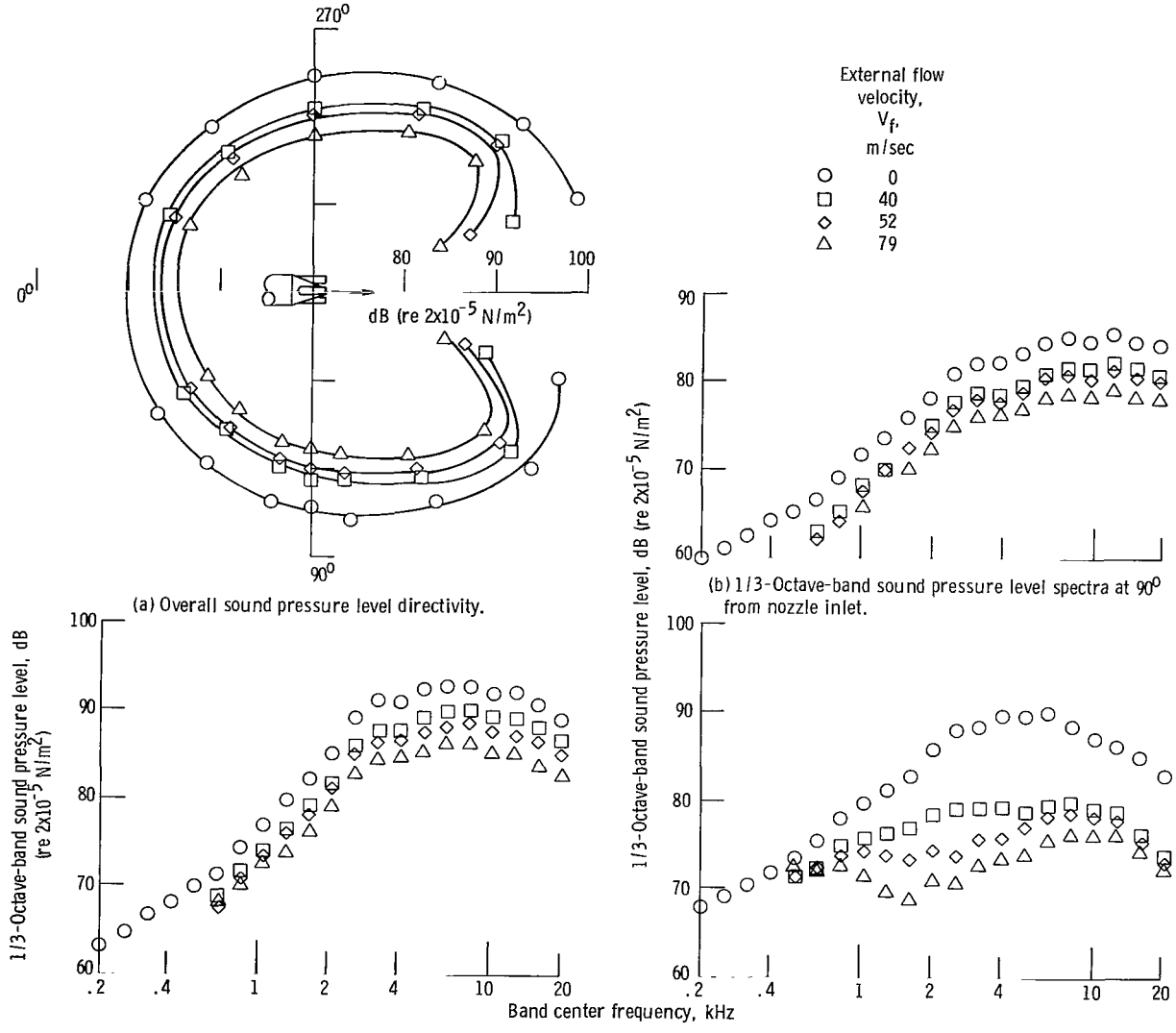

(a) Overall sound pressure level directivity.

(b) 1/3-Octave-band sound pressure level spectra at 90° from nozzle inlet.

(c) 1/3-Octave-band sound pressure level spectra at 140° from nozzle inlet.

(d) 1/3-Octave-band sound pressure level spectra at 160° from nozzle inlet.

Figure 29. - Effect of external flow on sound levels from eight-tube mixer nozzle alone. Nozzle jet velocity, V_j, 283 meters per second; microphone distance, 3.05 meters.

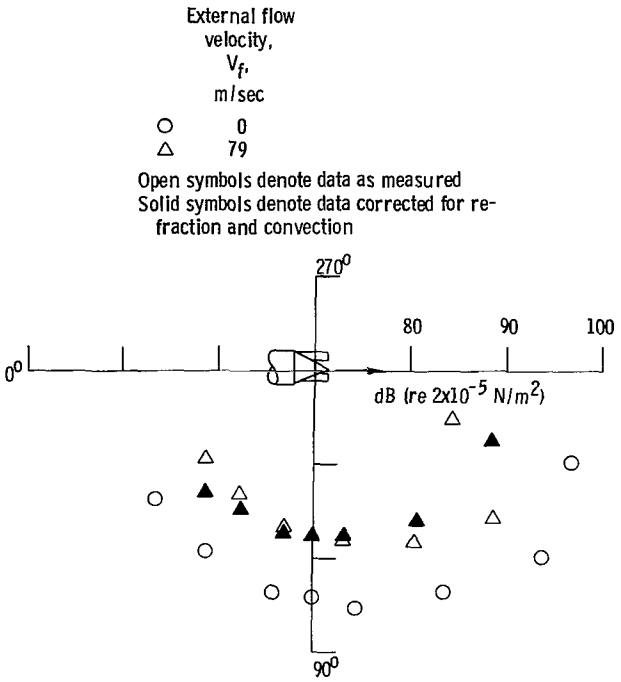

Figure 30. - Comparison of sound levels with and without corrections for refraction and convection for eight-tube mixer nozzle alone. Nozzle jet velocity, V_j, 283 meters per second; microphone distance, 3.05 meters.

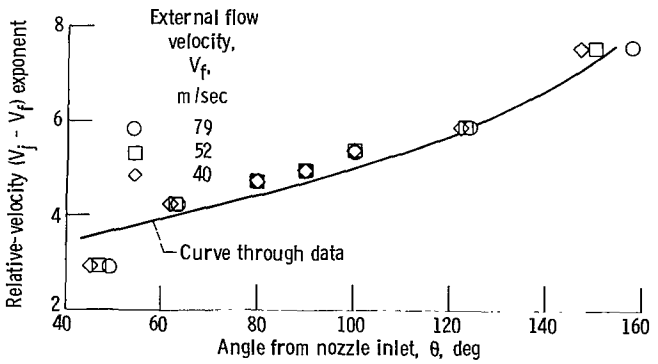

Figure 31. - Relative-velocity exponent as function of directivity angle for eight-tube mixer nozzle alone. Data corrected for refraction and convection.

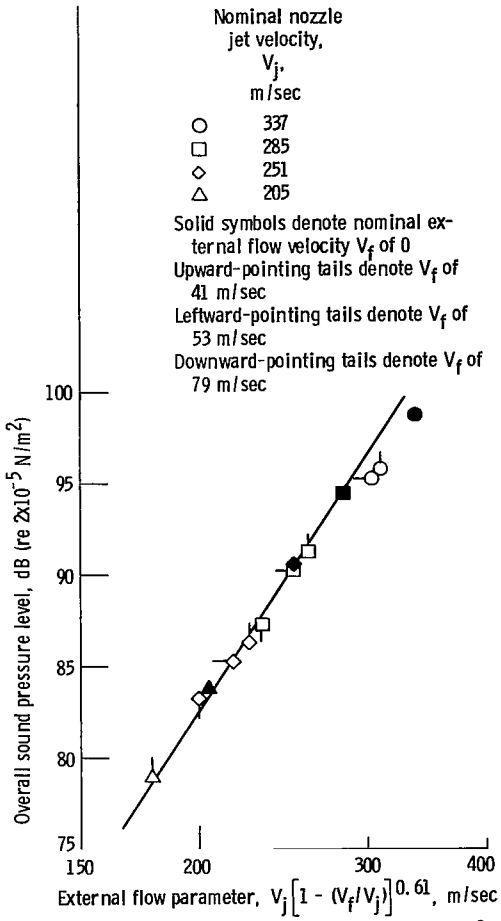

Figure 32. - Overall sound pressure level at 90° from nozzle inlet as function of an external flow parameter for eight-tube mixer nozzle alone. Microphone distance, 3.05 meters.

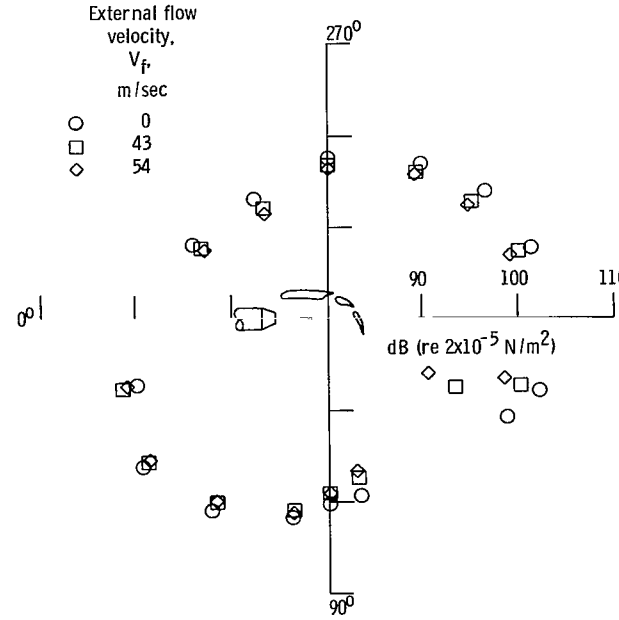

(a) Overall sound pressure level directivity.

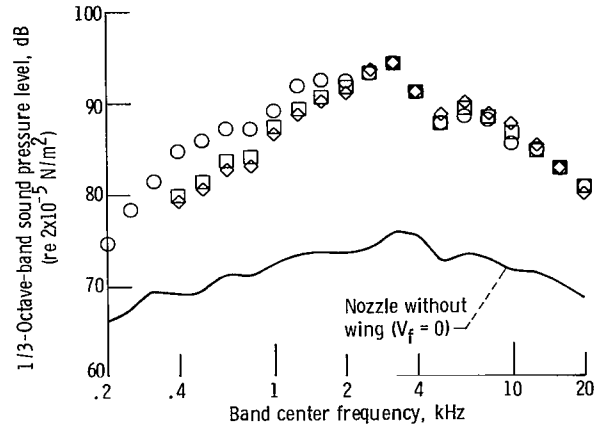

(b) 1/3-Octave-band sound pressure level spectra at 80° from nozzle inlet.

Figure 33. - Effect of external flow on sound levels for conical nozzle/wing with 30°-60° flap setting. Nozzle jet velocity, V_j, 208 meters per second; microphone distance, 3.05 meters.

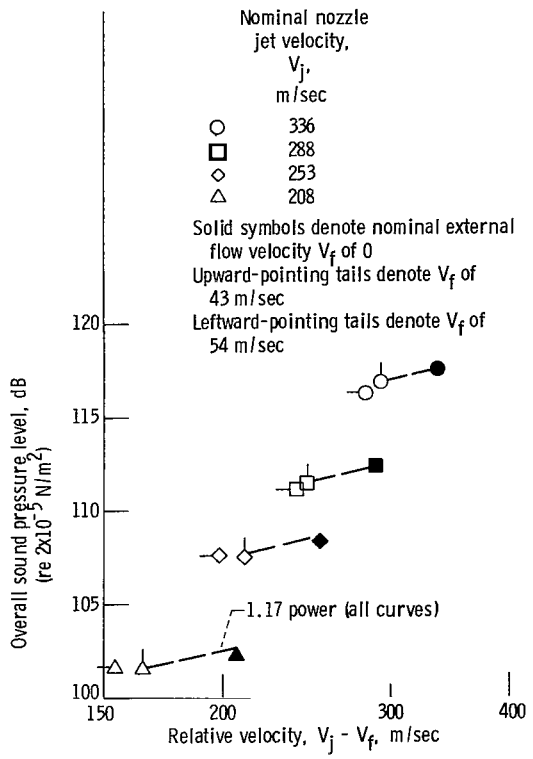

Figure 34. - Overall sound pressure level at 80° from nozzle inlet as function of relative velocity for conical nozzle/wing with 30°-60° flap setting. Microphone distance, 3.05 meters.

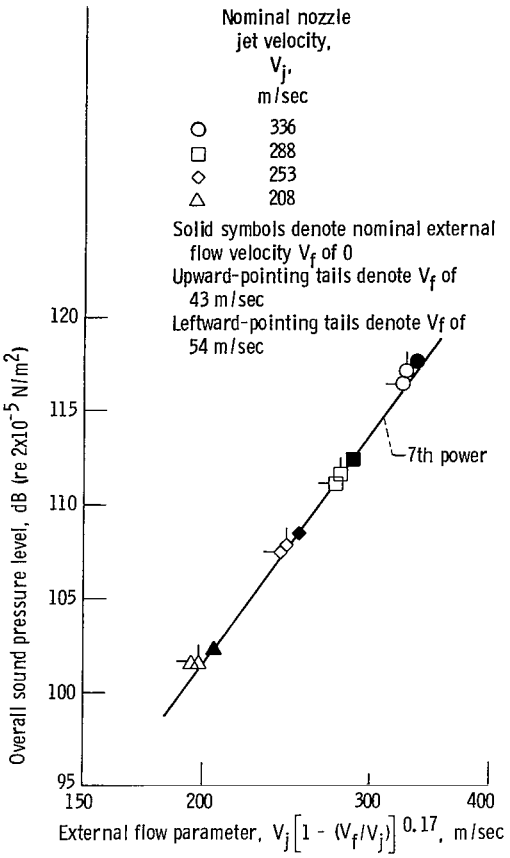

Figure 35. - Overall sound pressure level at 80° from nozzle inlet as function of an external flow parameter for conical nozzle/wing with 30°-60° flap setting. Microphone distance, 3.05 meters.

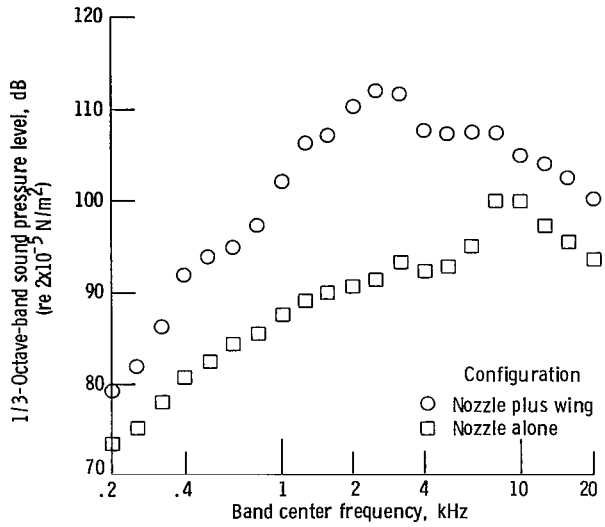

Figure 36. - Comparison of spectra at 80^{0} from nozzle inlet for conical nozzle/wing with 30^{0}-60^{0} flap setting and conical nozzle alone for supersonic jet velocity flow condition. No external flow; nozzle jet velocity, V_j, 336 meters per second; microphone distance, 3.05 meters.

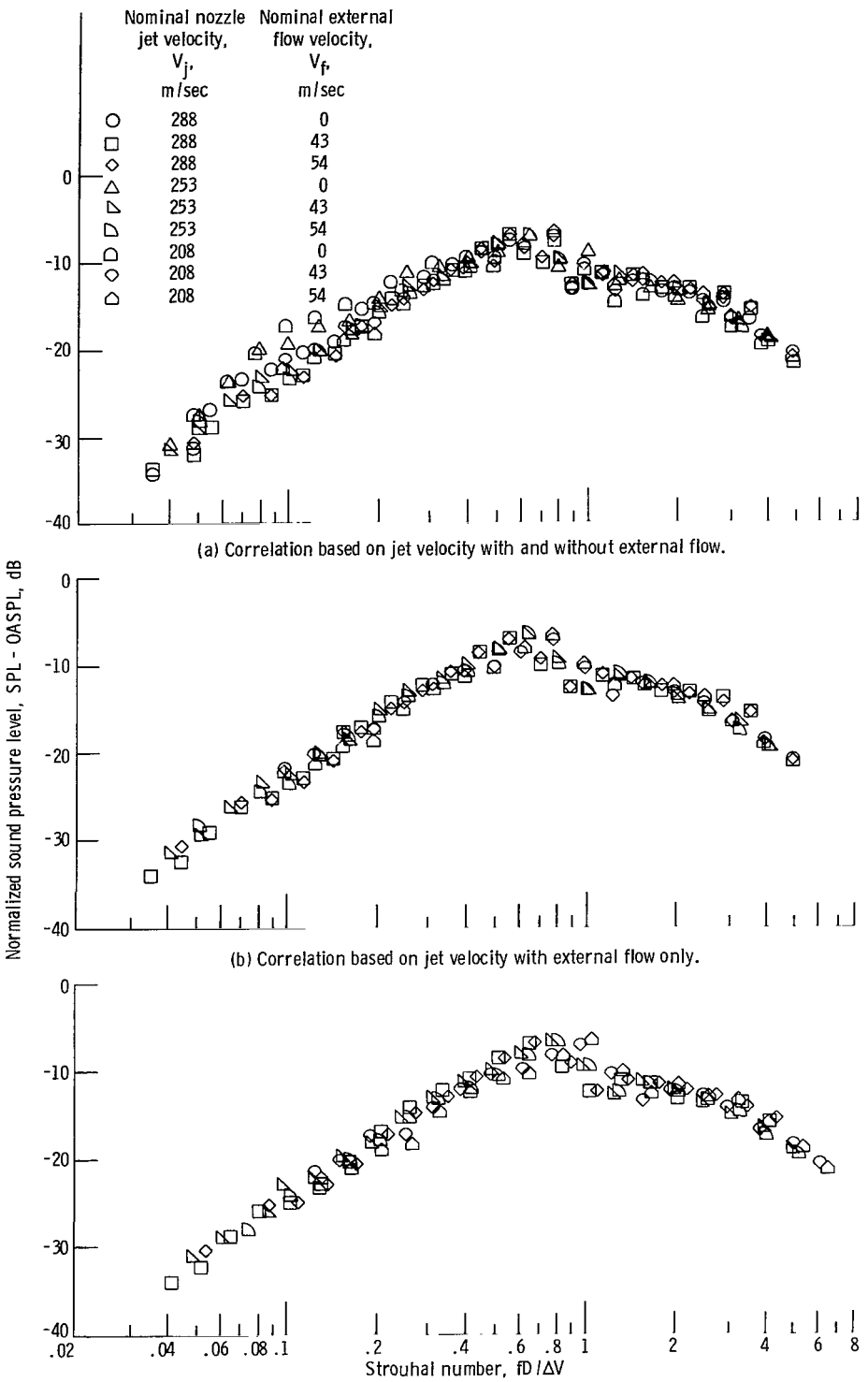

(a) Correlation based on jet velocity with and without external flow.

(b) Correlation based on jet velocity with external flow only.

(c) Correlation based on relative velocity.

Figure 37. - Normalized sound pressure level spectra for conical nozzle/wing with 30^0-60^0 flap setting. Angle from nozzle inlet, θ, 80^0; microphone distance, 3.05 meters.

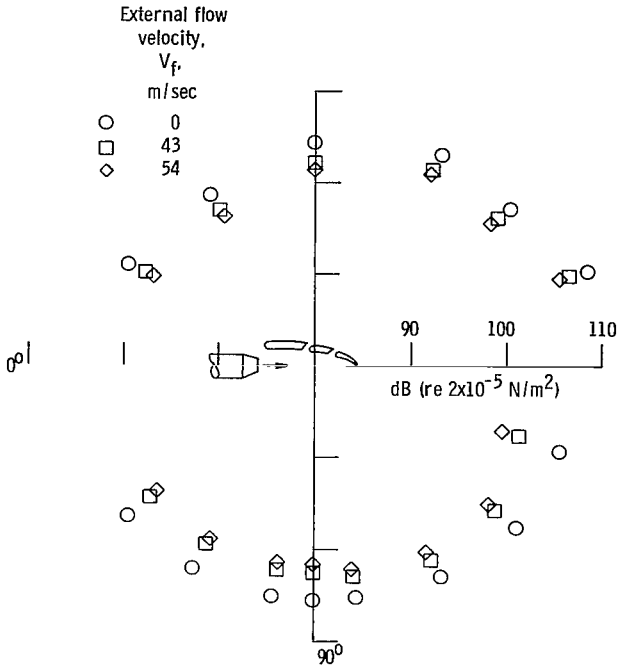

(a) Overall sound pressure level directivity.

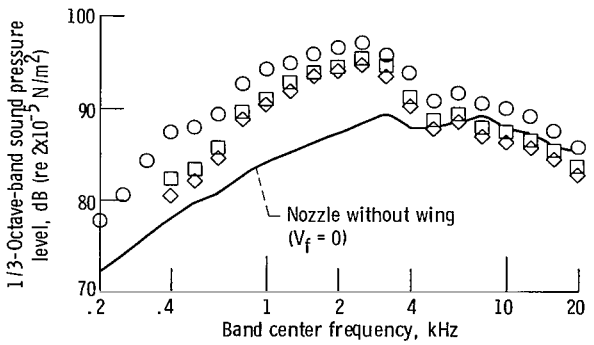

(b) 1/3-Octave-band sound pressure level spectra at 100° from nozzle inlet.

Figure 38. - Effect of external flow on sound levels for conical nozzle/wing with 10°-20° flap setting. Nozzle jet velocity, V_j, 291 meters per second; microphone distance, 3.05 meters.

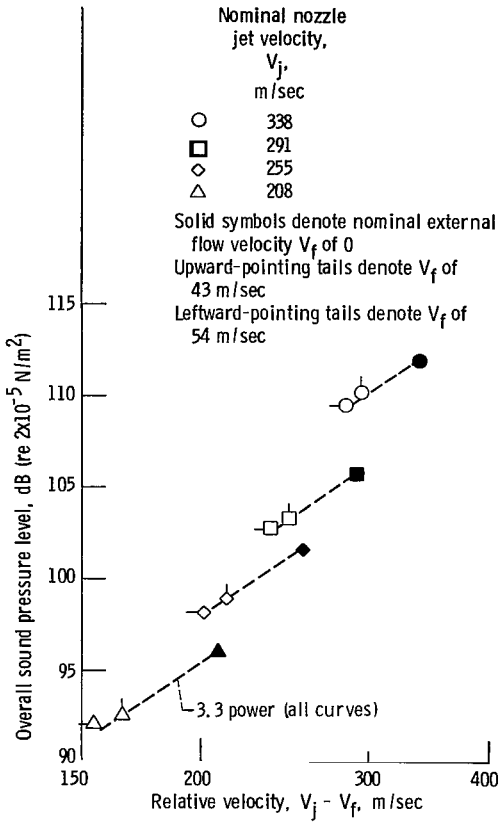

Figure 39. - Overall sound pressure level at 100° from nozzle inlet as function of relative velocity for conical nozzle/wing with 10°-20° flap setting. Microphone distance, 3.05 meters.

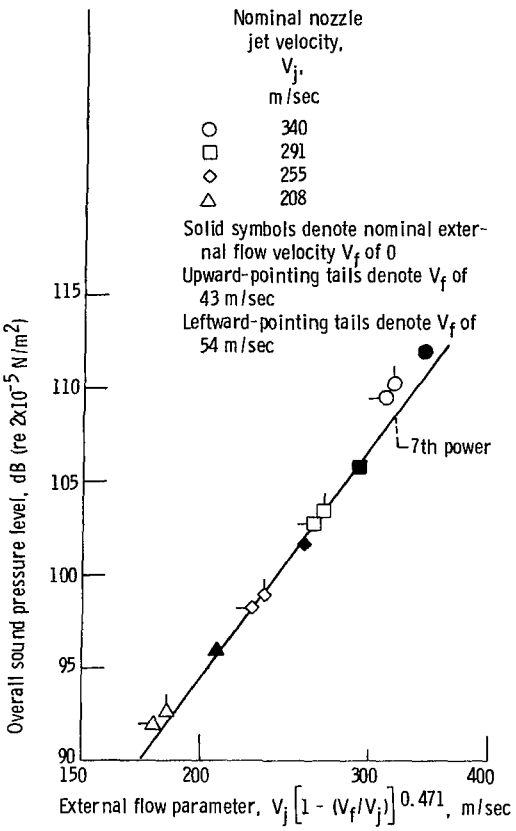

Figure 40. - Overall sound pressure level at 100° from nozzle inlet as function of an external flow parameter for conical nozzle/wing with 10°-20° flap setting. Microphone distance, 3.05 meters.

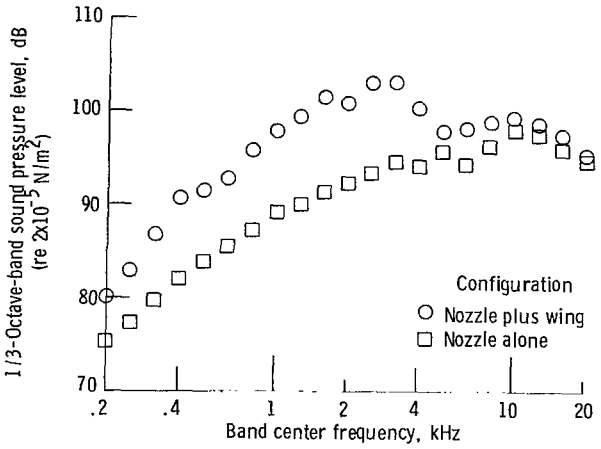

Figure 41. - Comparison of spectra at 100° from nozzle inlet for conical nozzle/wing with 10°-20° flap setting and conical nozzle alone for supersonic jet velocity condition. No external flow; nozzle jet velocity, 340 meters per second; microphone distance, 3.05 meters.

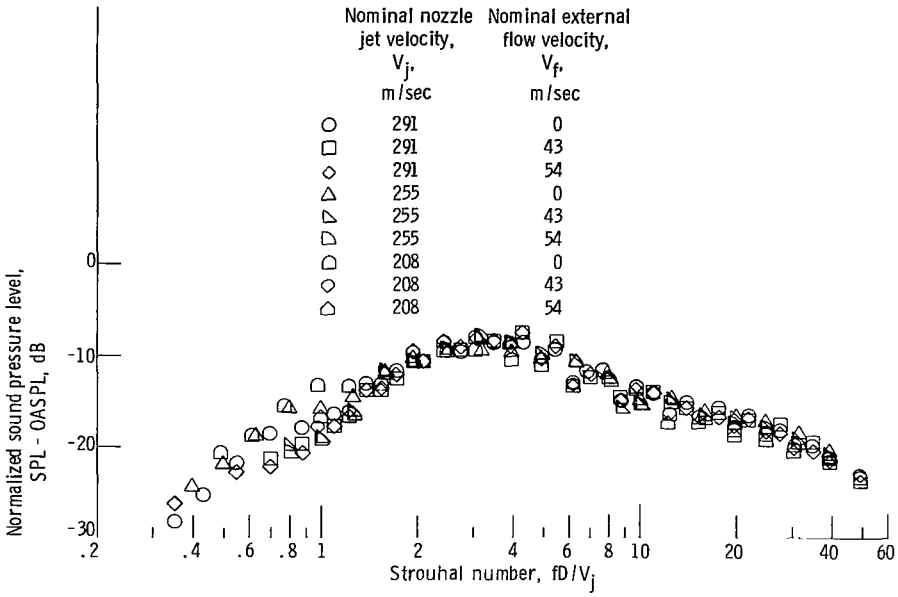

Figure 42. - Normalized sound pressure level spectra for conical nozzle/wing with 10^0-20^0 flap setting. Angle from nozzle inlet, θ, 100^0; microphone distance, 3.05 meters.

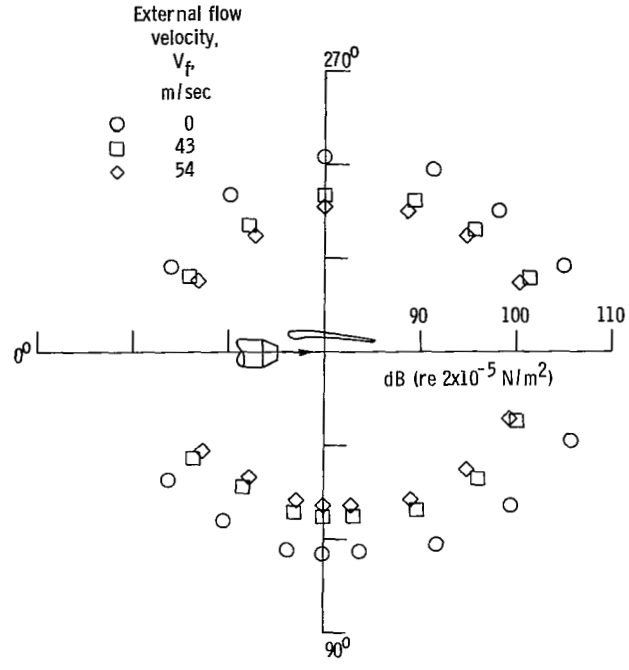

(a) Overall sound pressure level directivity.

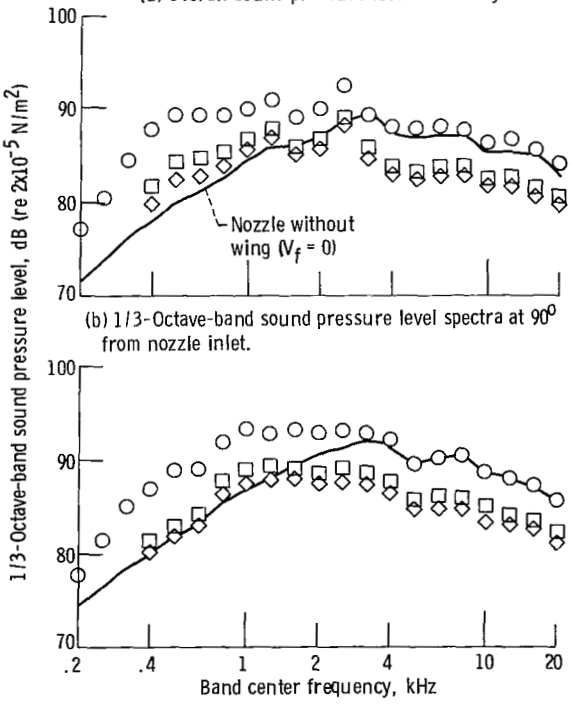

(b) 1/3-Octave-band sound pressure level spectra at 90° from nozzle inlet.

(c) 1/3-Octave-band sound pressure level spectra at 120° from nozzle inlet.

Figure 43. - Effect of external flow on sound levels for conical nozzle/wing with flaps retracted. Nozzle jet velocity, V_j, 290 meters per second; microphone distance, 3.05 meters.

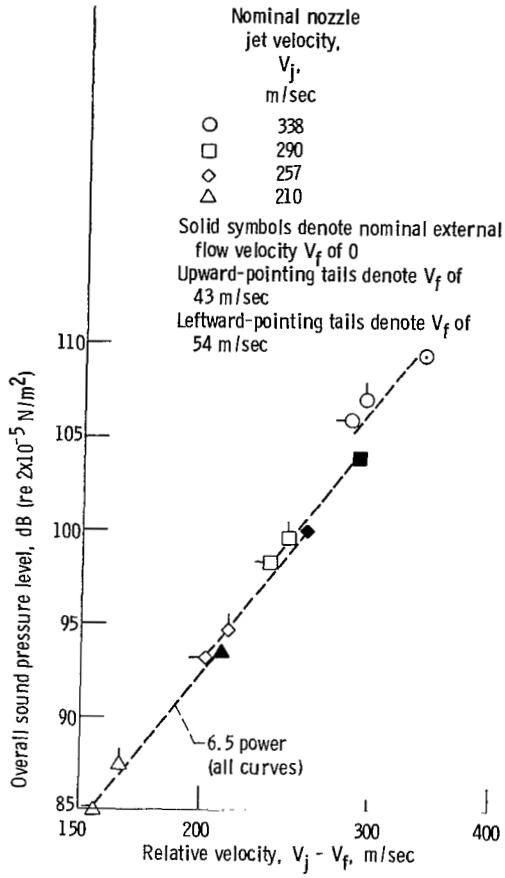

Figure 44. - Overall sound pressure level at 120° from nozzle inlet as function of relative velocity for conical nozzle/wing with flaps retracted. Microphone distance, 3.05 meters.

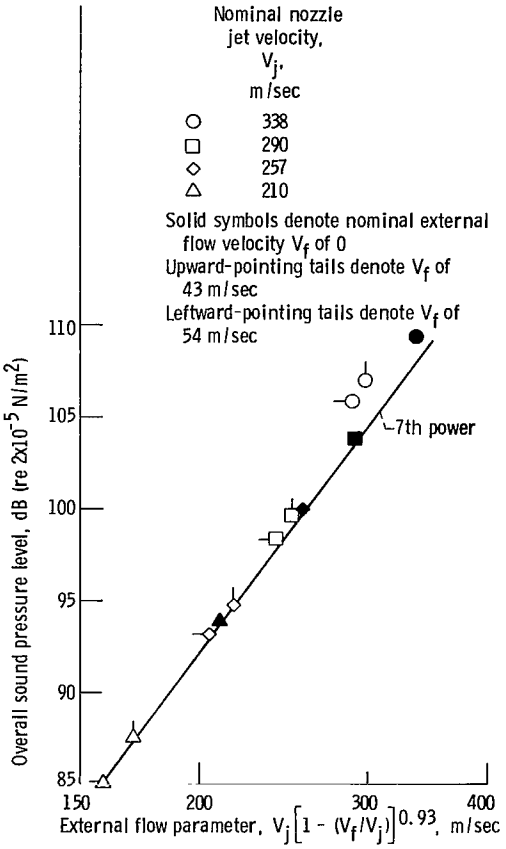

Figure 45. - Overall sound pressure level at 120° from nozzle inlet as function of an external flow parameter for conical nozzle/wing with flaps retracted. Microphone distance, 3.05 meters.

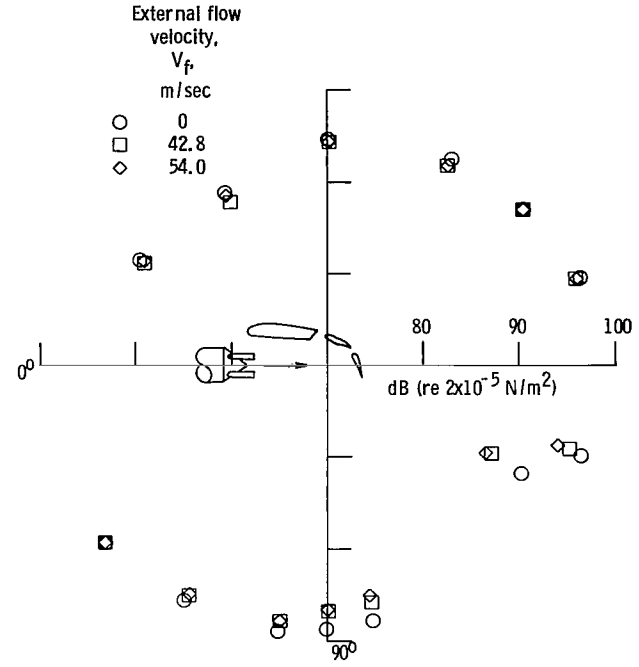

(a) Overall sound pressure level directivity.

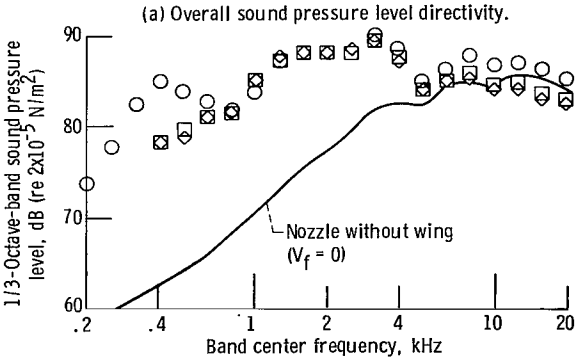

(b) 1/3-Octave-band sound pressure level spectra at 80° from nozzle inlet.

Figure 46. - Effect of external flow on sound levels for eight-tube mixer nozzle/wing with 30°-60° flap setting. Nozzle jet velocity, 292 meters per second; microphone distance, 3.05 meters.

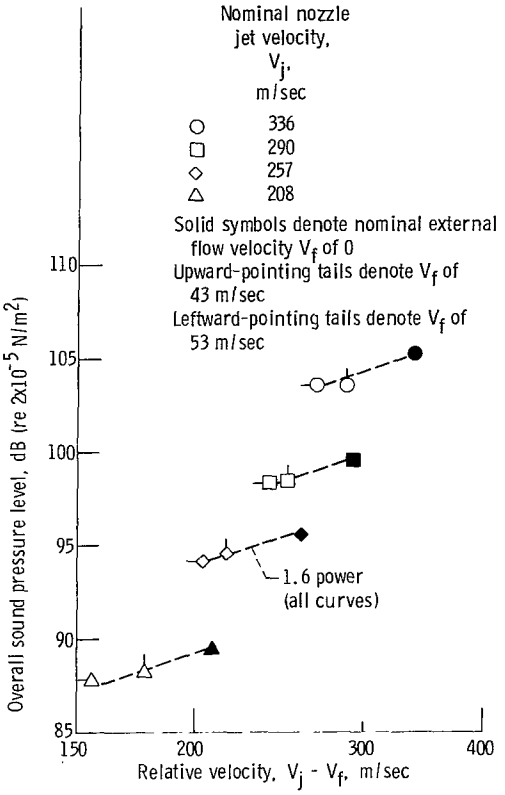

Figure 47. - Overall sound pressure level at 80° from nozzle inlet as function of relative velocity for eight-tube mixer nozzle/wing with flaps at 30°-60° setting. Microphone distance, 3.05 meters.

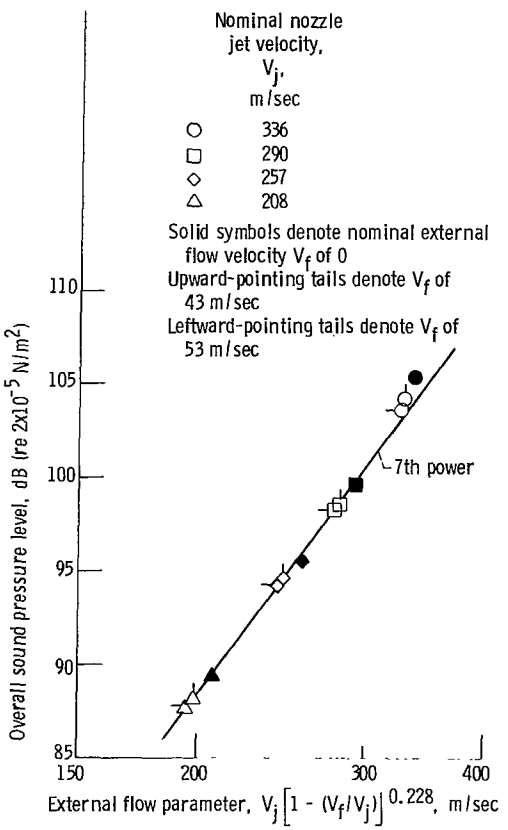

Figure 48. - Overall sound pressure level at 80° from nozzle inlet as function of an external flow parameter for eight-tube mixer nozzle/wing with 30°-60° flap setting. Microphone distance, 3.05 meters.

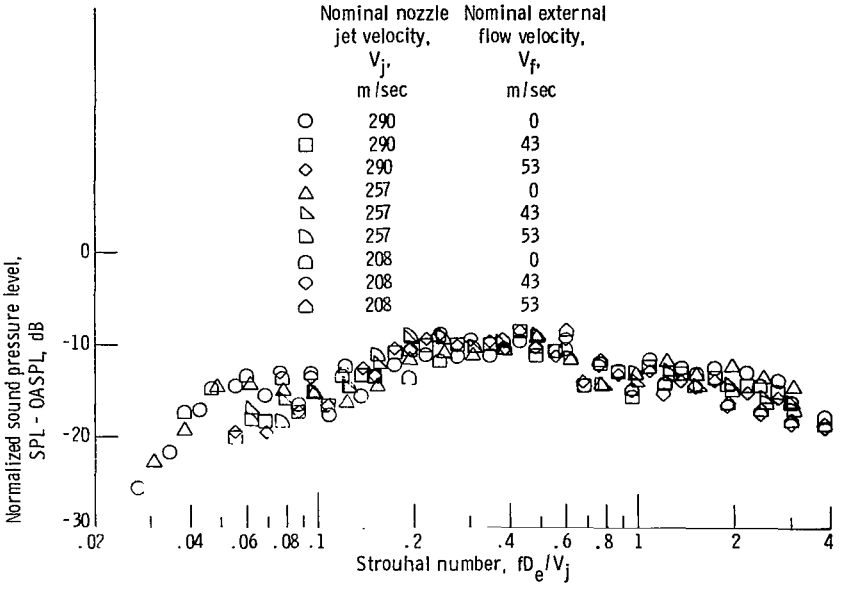

Figure 49. - Normalized sound pressure level spectra for mixer nozzle/wing with 30^0-60^0 flap setting. Angle from nozzle inlet, 80^0; microphone distance, 3.05 meters.

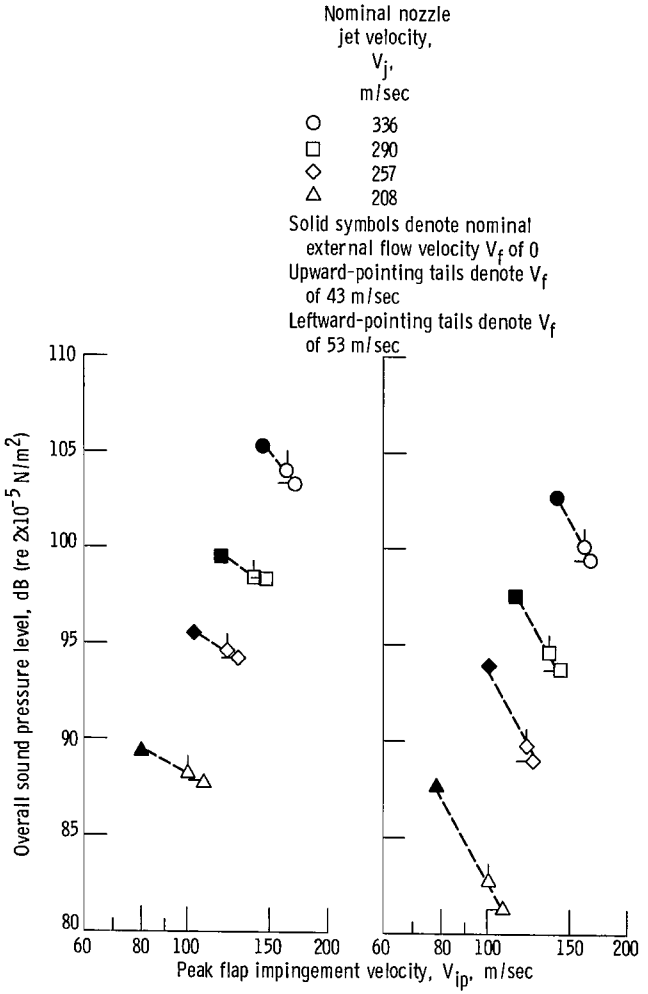

(a) Flap setting, 30^0-60^0; angle from nozzle inlet, θ, 80^0.

(b) Flap setting, 10^0-20^0; angle from nozzle inlet, θ, 100^0.

Figure 50. - Overall sound pressure level as function of peak flap impingement velocity for eight-tube mixer nozzle with wing. Microphone distance, 3.05 meters.

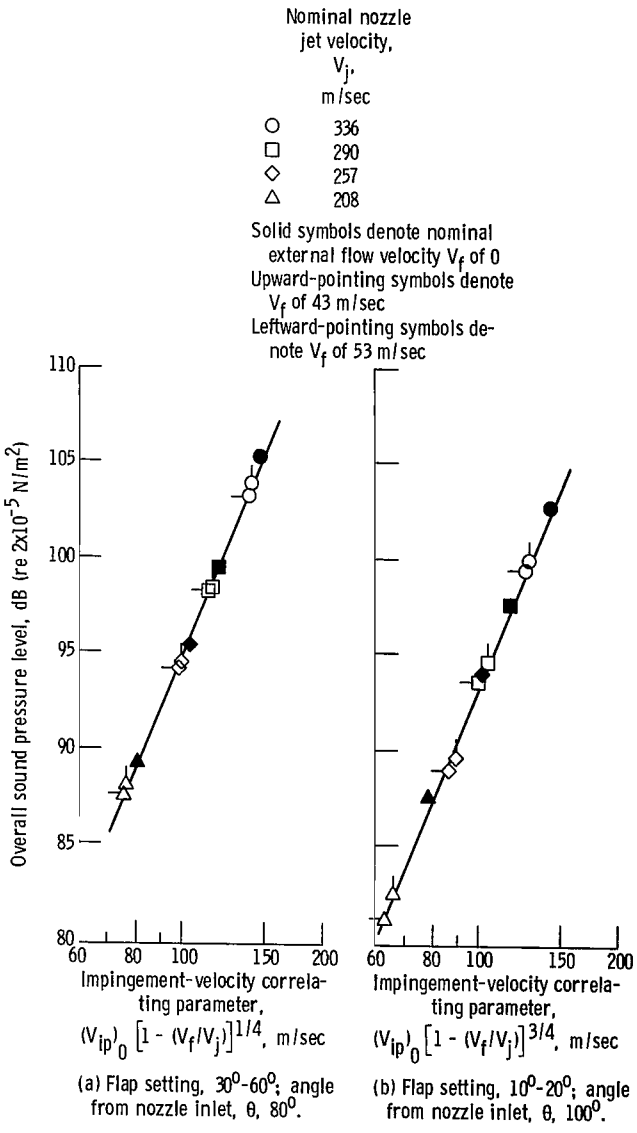

(a) Flap setting, 30^0-60^0; angle from nozzle inlet, θ, 80^0.

(b) Flap setting, 10^0-20^0; angle from nozzle inlet, θ, 100^0.

Figure 51. - Correlation of overall sound pressure level with flap impingement velocity for mixer nozzle/wing. Microphone distance, 3.05 meters.

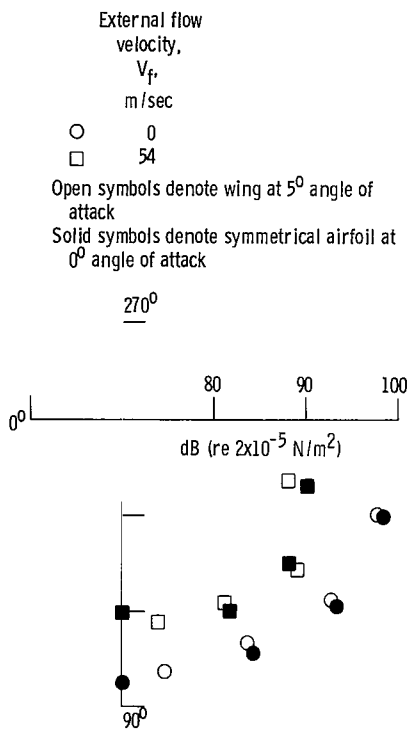

(a) Overall sound pressure level directivity.

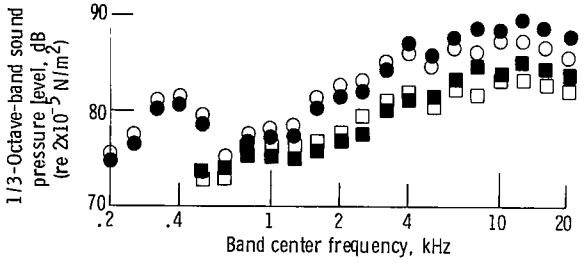

(b) 1/3-Octave-band sound pressure level spectra at 120° from nozzle inlet.

Figure 52. - Effect of wing-to-nozzle angle of attack on sound levels for eight-tube mixer nozzle/wing with flaps retracted. Nozzle jet velocity, V_j, 292 meters per second; microphone distance, 3.05 meters.

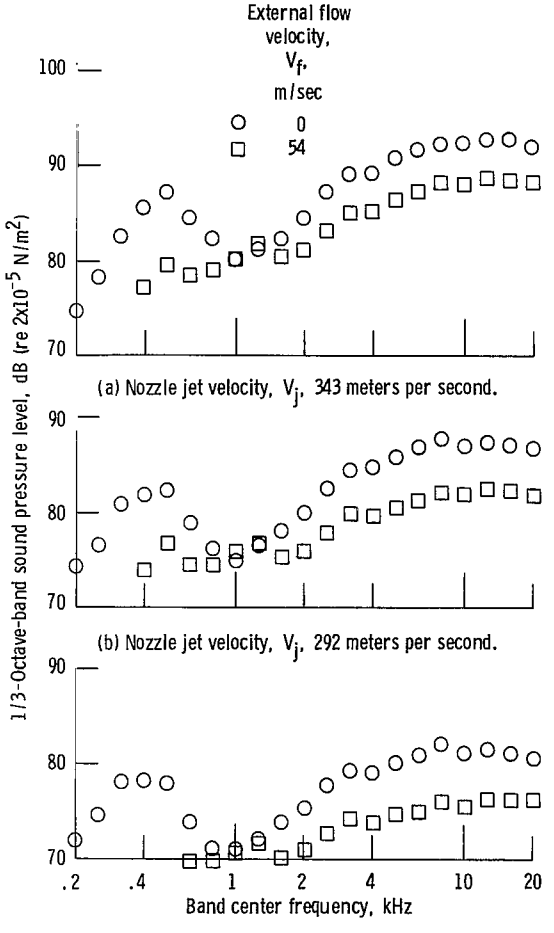

(a) Nozzle jet velocity, V_j, 343 meters per second.

(b) Nozzle jet velocity, V_j, 292 meters per second.

(c) Nozzle jet velocity, V_j, 259 meters per second.

Figure 53. - Comparison of effect of external flow on spectra at 90° from nozzle inlet for symmetrical airfoil at different jet velocities. Microphone distance, 3.05 meters.

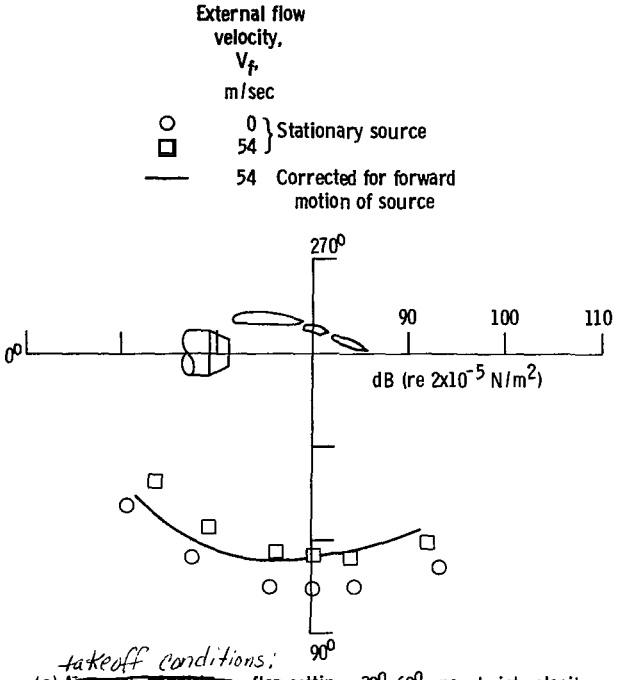

takeoff conditions:

(a) [redacted]: flap setting, 30°-60°; nozzle jet velocity, V_j, 207 meters per second.

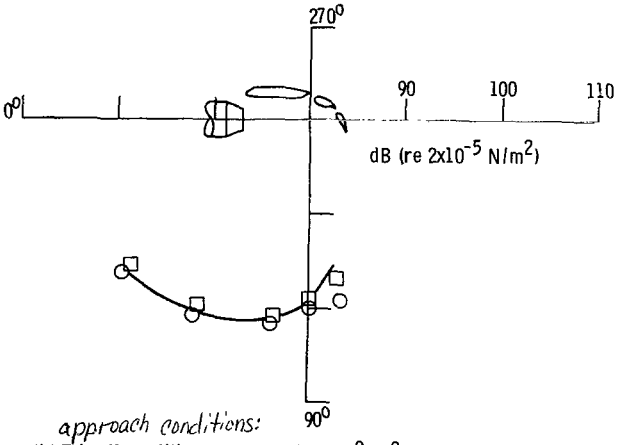

approach conditions:

(b) [redacted]: flap setting, 10°-20°; nozzle jet velocity, V_j, 291 meters per second.

Figure 54. - Flap noise radiation patterns showing calculated effect of forward motion of source. Conical nozzle; microphone distance, 3.05 meters.

NASA-Langley, 1976 E-8697

"The aeronautical and space activities of the United States shall be conducted so as to contribute . . . to the expansion of human knowledge of phenomena in the atmosphere and space. The Administration shall provide for the widest practicable and appropriate dissemination of information concerning its activities and the results thereof."

—NATIONAL AERONAUTICS AND SPACE ACT OF 1958

NASA SCIENTIFIC AND TECHNICAL PUBLICATIONS

TECHNICAL REPORTS: Scientific and technical information considered important, complete, and a lasting contribution to existing knowledge.

TECHNICAL NOTES: Information less broad in scope but nevertheless of importance as a contribution to existing knowledge.

TECHNICAL MEMORANDUMS: Information receiving limited distribution because of preliminary data, security classification, or other reasons. Also includes conference proceedings with either limited or unlimited distribution.

CONTRACTOR REPORTS: Scientific and technical information generated under a NASA contract or grant and considered an important contribution to existing knowledge.

TECHNICAL TRANSLATIONS: Information published in a foreign language considered to merit NASA distribution in English.

SPECIAL PUBLICATIONS: Information derived from or of value to NASA activities. Publications include final reports of major projects, monographs, data compilations, handbooks, sourcebooks, and special bibliographies.

TECHNOLOGY UTILIZATION PUBLICATIONS: Information on technology used by NASA that may be of particular interest in commercial and other non-aerospace applications. Publications include Tech Briefs, Technology Utilization Reports and Technology Surveys.

Details on the availability of these publications may be obtained from:

SCIENTIFIC AND TECHNICAL INFORMATION OFFICE

NATIONAL AERONAUTICS AND SPACE ADMINISTRATION

Washington, D.C. 20546